



**HAL**  
open science

# A nonstandard wave decomposition to ensure the convergence of Debye series for modeling wave propagation in an immersed anisotropic elastic plate

Eric Ducasse, Marc Deschamps

► **To cite this version:**

Eric Ducasse, Marc Deschamps. A nonstandard wave decomposition to ensure the convergence of Debye series for modeling wave propagation in an immersed anisotropic elastic plate. *Wave Motion*, 2012, 8 (745-764), pp.49. 10.1016/j.wavemoti.2012.05.001 . hal-00872329

**HAL Id: hal-00872329**

**<https://hal.science/hal-00872329>**

Submitted on 11 Oct 2013

**HAL** is a multi-disciplinary open access archive for the deposit and dissemination of scientific research documents, whether they are published or not. The documents may come from teaching and research institutions in France or abroad, or from public or private research centers.

L'archive ouverte pluridisciplinaire **HAL**, est destinée au dépôt et à la diffusion de documents scientifiques de niveau recherche, publiés ou non, émanant des établissements d'enseignement et de recherche français ou étrangers, des laboratoires publics ou privés.



## Science Arts & Métiers (SAM)

is an open access repository that collects the work of Arts et Métiers ParisTech researchers and makes it freely available over the web where possible.

This is an author-deposited version published in: <http://sam.ensam.eu>  
Handle ID: <http://hdl.handle.net/10985/7388>

### To cite this version :

Eric DUCASSE, Marc DESCHAMPS - A nonstandard wave decomposition to ensure the convergence of Debye series for modeling wave propagation in an immersed anisotropic elastic plate - Wave Motion - Vol. 8, n°745-764, p.49 - 2012

Any correspondence concerning this service should be sent to the repository

Administrator : [archiveouverte@ensam.eu](mailto:archiveouverte@ensam.eu)

# A nonstandard wave decomposition to ensure the convergence of Debye series for modeling wave propagation in an immersed anisotropic elastic plate

Eric Ducasse<sup>1,2,3,4</sup> [e.ducasse@i2m.u-bordeaux1.fr](mailto:e.ducasse@i2m.u-bordeaux1.fr)

Marc Deschamps<sup>3,2</sup> [m.deschamps@i2m.u-bordeaux1.fr](mailto:m.deschamps@i2m.u-bordeaux1.fr)

<sup>1</sup> Arts et Metiers ParisTech, *I<sub>2</sub>M-APy*, UMR 5295, F-33400 Talence, France.

<sup>2</sup> Univ. Bordeaux, *I<sub>2</sub>M-APy*, UMR 5295, F-33400 Talence, France.

<sup>3</sup> CNRS, *I<sub>2</sub>M-APy*, UMR 5295, F-33400 Talence, France.

<sup>4</sup> Corresponding author. Tel. +33(0)540003138. Fax +33(0)540006964.

## Abstract

When ultrasonic guided waves in an immersed plate are expressed as Debye series, they are considered as the result of successive reflections from the plate walls. Against all expectations, the Debye series can diverge for any geometry if inhomogeneous waves are involved in the problem. For an anisotropic elastic plate immersed in a fluid, this is the case if the incidence angle is greater than the first critical angle.

Physically, this divergence can be explained by the energy coupling between two inhomogeneous waves of same kind of polarization, which are expressed by conjugate wavenumbers. Each of these latter inhomogeneous waves does not transfer energy but a linear combination of them can do it. Mathematically, this is due to the fact that inhomogeneous waves do not constitute a basis orthogonal in the sense of energy, contrarily to homogeneous waves. To avoid that difficulty, an orthogonalization of these inhomogeneous waves is required. Doing so, *nonstandard upgoing and downgoing waves* in the plate are introduced to ensure the convergence of the new Debye series written in the basis formed by these latter waves.

The case of an aluminum plate immersed in water illustrates this study by giving numerical results and a detailed description of the latter nonstandard waves. The different reflection and refraction coefficients at each plate interface are analyzed in terms of Debye series convergence and of distribution of energy fluxes between the waves in the plate. From that investigation, an interesting physical phenomenon is described for one specific pair “*angle of incidence/frequency*”. For this condition, the quasi-energy brought by the incident harmonic plane wave crosses the plate without any conversion to reflected waves either at the first interface or at the second interface. In this zone, there is a perfect impedance matching between the fluid and the plate.

## Keywords

Ultrasonic wave scattering; Immersed plate; Debye series; Nonstandard wave; Energy-flux direction.

# 1 Introduction

The propagation of elastic waves in an elastic layer sandwiched between two half-spaces can be modeled by using Debye series [1], *i.e.* the total field is considered as the result of multiple reflections/refractions [2][3] at the interfaces. This technique has been fruitfully used for elastic cylindrical rods [4][5], for spherical elastic layers [6], and for plates [7][8][9].

Unfortunately, the Debye series can diverge for any geometry if inhomogeneous waves are involved in the problem. For an anisotropic elastic plate immersed in a fluid (*cf.* Fig 1), this is the case if the incidence angle is greater than the first critical angle (see for example [7]). Physically, this divergence can be explained by the energy coupling between two inhomogeneous waves of same kind of polarization, which are expressed by conjugate wavenumbers. Each of these latter inhomogeneous waves does not transfer energy but a linear combination of them can do it. Mathematically, this is due to the fact that inhomogeneous waves do not constitute a basis orthogonal in the sense of energy, contrarily to homogeneous waves.

To avoid that difficulty, an orthogonalization of these inhomogeneous waves is required. Doing so, *upgoing and downgoing waves* in the plate are defined differently than the usual way. It is then shown that using these *nonstandard progressive waves* ensures the convergence of the Debye series. Consequently, in our knowledge, this provides an efficient solution to an old unresolved problem.

In the first part, the theoretical background for modeling a layer sandwiched between two half-spaces by Debye series is reminded. In the second part, the study of the multiple reflections/refractions, in terms of energy, is done in the case of the more general anisotropic elastic plates. It is emphasized that the Debye series can diverge when using the usual exponential upgoing and downgoing solutions, and that the orthogonalization, in the sense of energy, of such wave basis yields the convergence of the series. Finally, the case of an aluminum plate immersed in water illustrates this study by giving numerical results. From an investigation of the reflection and refraction coefficients at the two interfaces, it is shown how their values, which depend on the choice of the orthogonal basis, influence the Debye series convergence and the interferences within the plate. In particular, an interesting physical phenomenon is described for one specific pair “*angle of incidence/frequency*”. For this condition, the quasi-energy brought by the incident harmonic plane wave crosses the plate without any conversion to reflected waves either at the first interface or at the second interface. In this zone, there is a perfect impedance matching between the fluid and the plate.

## 2 Principles of Debye series modeling

An anisotropic elastic plate, parallel to the  $xy$ -plane and perpendicular to the  $z$ -direction, is immersed in a fluid and insonified by a time-harmonic plane wave of incidence angle  $\theta$  and angular frequency  $\omega$ , the propagation direction being in the  $xz$ -plane (*cf.* Fig 1). The received energy is firstly converted into elastodynamic waves in the plate and then released to the fluid above (reflected wave) and below (transmitted wave). The so-called “Debye series modeling” consists in writing the elastodynamic field in the plate as the sum of downgoing and upgoing waves successively reflected at each interface. The energy is progressively released to the fluid at each reflection/refraction.

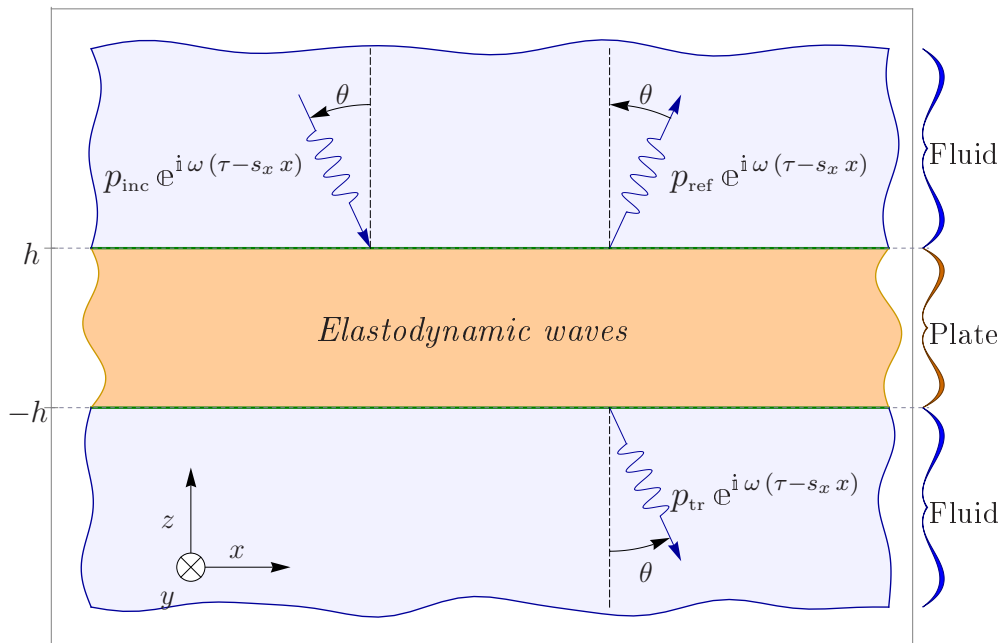


Figure 1: An elastic plate immersed in a fluid, insonified by a plane wave of incidence angle  $\theta$ .

## 2.1 Theoretical background

### 2.1.1 Incident and reflected field

The incident (downgoing) time-harmonic plane wave in the fluid is characterized by the acoustic pressure  $p_{\text{inc}}(z) \exp[i\omega(\tau - s_x x)]$ , where:

$$p_{\text{inc}}(z) = a_{\text{inc}} \sqrt{\frac{2s_z}{\rho}} \exp[i\omega s_z(z - h)] = a_{\text{inc}} \sqrt{\frac{2s_z}{\rho}} \exp[i s_z(z - H)], \quad z > h, \quad (1)$$

$\tau$  denoting time,  $s_x = \sin(\theta)/c$  the slowness in the  $x$ -direction,  $s_z = \cos(\theta)/c$  the slowness in the  $z$ -direction,  $c$  the sound velocity in the fluid,  $\rho$  the density,  $2h$  the thickness of the plate,  $z = \omega z$  and  $H = \omega h$  frequency-position products. The coefficient  $\sqrt{2s_z/\rho}$  is due to normalization with respect to the mean power flux in the  $z$ -direction, that is, the mean power flux is negative and equal to  $-|a_{\text{inc}}|^2$ .

Due to the Snell-Descartes law related to the reflection/refraction of the harmonic plane wave of this study, the factor  $\exp[i\omega(\tau - s_x x)]$ , containing the dependence with respect to time  $\tau$  and abscissa  $x$ , necessarily appears in all expressions of acoustic fields. Hence, the latter factor will be then omitted below.

Thus, the reflected (upgoing) field is given by:

$$p_{\text{ref}}(z) = a_{\text{ref}} \sqrt{\frac{2s_z}{\rho}} \exp[-i s_z(z - H)], \quad z > h, \quad (2)$$

and its mean power flux in the  $z$ -direction is positive and equal to  $|a_{\text{ref}}|^2$ .

### 2.1.2 Transmitted field

The transmitted (downgoing) field in the fluid below the plate is characterized by:

$$p_{\text{tr}}(z) = a_{\text{tr}} \sqrt{\frac{2s_z}{\rho}} \exp[i s_z(z + H)], \quad z < -h. \quad (3)$$

and its mean power flux in the  $z$ -direction is negative and equal to  $-|a_{\text{tr}}|^2$ .

### 2.1.3 Plate vibration

By using Stroh sextic formalism (*e.g.*, [10], [11], [12], [13], [14]), the vibrational state of the elastic anisotropic plate is described by the following six-dimensional vector:

$$\mathbf{U}(z) = \begin{bmatrix} \mathbf{v}(z) \\ \boldsymbol{\sigma}_z(z) \end{bmatrix}, \quad -h < z < h, \quad (4)$$

where  $\mathbf{v}$  is the velocity vector and  $\boldsymbol{\sigma}_z$  the stress in the  $z$ -direction.

Note that this six-dimensional vector is not the most commonly used, the latter containing the displacement vector ( $-\mathrm{i}\omega^{-1}\mathbf{v}$ ) and the vector ( $\mathrm{i}\omega^{-1}s_x^{-1}\boldsymbol{\sigma}_z$ ) (*e.g.*, [11], [15], [16]).

The state vector  $\mathbf{U}$  can be expressed as follows:

$$\mathbf{U}(z) = \mathcal{N}(z) \mathbf{a} = \Xi \mathcal{E}(z) \mathbf{a}, \quad (5)$$

where the matrix  $\Xi = \left( \begin{array}{c|c} \boldsymbol{\xi}_1 & \cdots & \boldsymbol{\xi}_6 \end{array} \right)$  contains the six-dimensional polarization vectors such that  $\boldsymbol{\xi}_\alpha = \left( \begin{array}{c|c} \mathbf{v}_\alpha^\top & \boldsymbol{\tau}_\alpha^\top \end{array} \right)^\top$ . The polarization vectors  $\mathbf{v}_\alpha$  and  $\boldsymbol{\tau}_\alpha$  are related to the velocity field and the stress field in the  $z$ -direction, respectively. The diagonal matrix  $\mathcal{E}(z) = \text{diag}[\exp(-\mathrm{i}\varsigma_\alpha z)]_{1 \leq \alpha \leq 6}$  represents the propagation,  $\varsigma_\alpha$  denoting the slowness in the  $z$ -direction. The six pairs  $(\varsigma_\alpha, \boldsymbol{\xi}_\alpha)_{1 \leq \alpha \leq 6}$  are the solutions of the following eigenvalue equation:

$$\mathcal{S} \boldsymbol{\xi}_\alpha = \varsigma_\alpha \boldsymbol{\xi}_\alpha, \quad (6)$$

where  $\mathcal{S}$  is the real-valued Stroh matrix defined by:

$$\mathcal{S} = \left\{ \begin{array}{c|c} -s_x (\mathbf{n} \diamond \mathbf{n})^{-1} (\mathbf{n} \diamond \mathbf{m}) & -(\mathbf{n} \diamond \mathbf{n})^{-1} \\ \hline s_x^2 [(\mathbf{m} \diamond \mathbf{m}) - (\mathbf{m} \diamond \mathbf{n}) (\mathbf{n} \diamond \mathbf{n})^{-1} (\mathbf{n} \diamond \mathbf{m})] - \rho_0 \mathbb{I}_3 & -s_x (\mathbf{m} \diamond \mathbf{n}) (\mathbf{n} \diamond \mathbf{n})^{-1} \end{array} \right\}, \quad (7)$$

which depends on the elasticity stiffness tensor, the density  $\rho_0$ , the slowness  $s_x$  and the unit vectors  $\mathbf{m}$  and  $\mathbf{n}$  of the  $x$  and  $z$  axes, respectively.

Indeed, the diamond  $\diamond$  bilinear product of two vectors  $\mathbf{a} = (a_1, a_2, a_3)^\top$  and  $\mathbf{b} = (b_1, b_2, b_3)^\top$ , associated with the elastic stiffness tensor  $(c_{ijklm})$ , is the matrix  $(\mathbf{a} \diamond \mathbf{b})$  such that  $(\mathbf{a} \diamond \mathbf{b})_{im} = c_{ijklm} a_j b_k$ , with the Einstein summation notation. This bilinear product has been already introduced by Lothe and Barnett in 1976 [11], but with the notation  $(ab)$ . We prefer the notation  $(\mathbf{a} \diamond \mathbf{b})$  to avoid any ambiguity with the product of two numbers  $a$  and  $b$ . Furthermore, this bilinear product has been applied in the literature to unit vectors only whereas it can be used with other vectors. Such notation is of interest to obtain compact expressions of different physical quantities, as will be emphasized in the next section [see for example Eq. (35)].

The symmetry properties of the elastic stiffness tensor implies that ([11] and [17]):

$$(\mathbf{b} \diamond \mathbf{a}) = (\mathbf{a} \diamond \mathbf{b})^\top \quad \text{and} \quad (\mathbf{a} \diamond \mathbf{b}) \mathbf{d} = (\mathbf{a} \diamond \mathbf{d}) \mathbf{b}. \quad (8)$$

In addition, for any non-zero real vector  $\mathbf{a}$ , the square matrix  $(\mathbf{a} \diamond \mathbf{a})$  is symmetric positive-definite [11].

The eigenvalue problem (6) admits real solutions, *i.e.*  $\varsigma_\alpha$  and  $\boldsymbol{\xi}_\alpha$  are real, and pairs of complex conjugate solutions, *i.e.*  $\varsigma_{\alpha+3} = \varsigma_\alpha^*$  and  $\boldsymbol{\xi}_{\alpha+3} = \boldsymbol{\xi}_\alpha^*$ , where the superscript  $*$  denotes the complex conjugation. They correspond to homogeneous (or bulk) waves and *conjugate* inhomogeneous (or surface) waves, respectively.

### 2.1.4 The scattering problem to solve

The continuity of normal component of the velocity vector and normal stress vector at each interface yields the following 4-by-8 systems of equations:

$$\mathbb{K} \underbrace{\mathcal{N}(H)}_{\mathbf{U}(H)} \mathbf{a} = \underbrace{a_{\text{inc}}}_{p_{\text{inc}}(H)} \mathbf{h}_{\text{down}} + \underbrace{a_{\text{ref}}}_{p_{\text{ref}}(H)} \mathbf{h}_{\text{up}}, \quad (9)$$

at the top edge of the plate, and:

$$\mathbb{K} \underbrace{\mathcal{N}(-H)}_{\mathbf{U}(-H)} \mathbf{a} = \underbrace{a_{\text{tr}}}_{p_{\text{tr}}(-H)} \mathbf{h}_{\text{down}}, \quad (10)$$

at its bottom edge. The matrix  $\mathbb{K}$  and the vectors  $\mathbf{h}_{\text{up}}$ ,  $\mathbf{h}_{\text{down}}$  are defined by:

$$\mathbb{K} = \begin{pmatrix} 0 & 0 & 1 & 0 & 0 & 0 \\ 0 & 0 & 0 & 1 & 0 & 0 \\ 0 & 0 & 0 & 0 & 1 & 0 \\ 0 & 0 & 0 & 0 & 0 & 1 \end{pmatrix}, \quad \mathbf{h}_{\text{up}} = \begin{pmatrix} \sqrt{2 s_z / \rho} \\ 0 \\ 0 \\ -\sqrt{2 \rho / s_z} \end{pmatrix}, \quad \mathbf{h}_{\text{down}} = \begin{pmatrix} -\sqrt{2 s_z / \rho} \\ 0 \\ 0 \\ -\sqrt{2 \rho / s_z} \end{pmatrix}, \quad (11)$$

Hence, in each expression, the first row corresponds to the normal component of the velocity vector and the last three rows give the normal components of the stress. Equations (9) and (10) constitute a eight-by-eight linear system with unknowns being the two coefficients  $a_{\text{ref}}$  (reflected wave above the plate) and  $a_{\text{tr}}$  (transmitted wave below the plate), and the six components of the vector  $\mathbf{a}$  associated with the six elastodynamic waves in the plate.

Linearity implies that:

$$a_{\text{ref}} = r a_{\text{inc}}, \quad a_{\text{tr}} = t a_{\text{inc}} \quad \text{and} \quad \mathbf{a} = a_{\text{inc}} \mathbf{g}. \quad (12)$$

Consequently, the problem consists in finding the reflection coefficient  $r$ , the transmission coefficient  $t$  and the vector  $\mathbf{g}$  which are transfer functions characterizing the response of the fluid/plate system. Omitting the material dependence, these transfer functions only depend on the incidence angle  $\theta$  and the frequency-half-thickness product  $H$ . Though they can be directly determined by solving Eqs. (9) and (10), it can be interesting to consider the total field in the plate as the result of successive reflections, notably in the time domain when we focus only on the first echoes. Furthermore, the latter transfer functions may have poles corresponding to Rayleigh-Lamb waves (*e.g.*, [18]), which can lead to numerical difficulties. The Debye series formulation may be an alternative to overcome these problems. Hence, the present paper focuses on this formulation involving successive reflections/refractions at the interfaces, as detailed in the next section and drawn in Fig. 2.

## 2.2 Successive reflections/refractions

The purpose of this section is to introduce notations useful in the next sections by recalling the classical decomposition of a field as the result of successive reflections/refractions.

### 2.2.1 Upgoing and downgoing waves in the plate

As detailed below in Section 3, the state vector  $\mathbf{U}(z)$  can be considered as the superposition of an upgoing wave  $\mathbf{U}_{\text{up}}(z)$  and a downgoing wave  $\mathbf{U}_{\text{down}}(z)$ :

$$\mathbf{U}(z) = \mathcal{N}(z) \begin{pmatrix} \mathbf{a}_{\text{up}} \\ \mathbf{a}_{\text{down}} \end{pmatrix} = \underbrace{\mathcal{N}_{\text{up}}(z) \mathbf{a}_{\text{up}}}_{\mathbf{U}_{\text{up}}(z)} + \underbrace{\mathcal{N}_{\text{down}}(z) \mathbf{a}_{\text{down}}}_{\mathbf{U}_{\text{down}}(z)}, \quad (13)$$

where  $\mathbf{a}_{\text{up,down}}$  are three-dimensional vectors, and  $\mathcal{N}_{\text{up,down}}(z)$  six-by-three matrices.

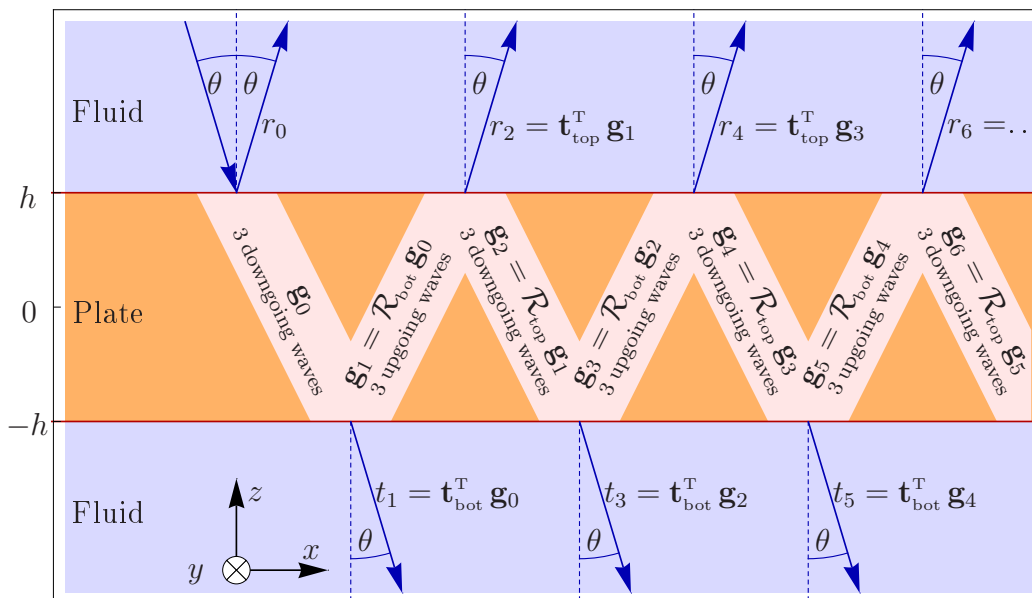


Figure 2: Successive reflections/refractions in an immersed plate.

### 2.2.2 The first reflection/refraction at the upper interface

The downgoing incident wave characterized by the coefficient  $a_{\text{inc}}$  gives an upgoing reflected acoustic wave in the fluid  $(a_{\text{inc}} r_0) \exp[-i s_z (z - H)]$  and a downgoing transmitted elastodynamic wave  $\mathcal{N}_{\text{down}}(z) (a_{\text{inc}} \mathbf{g}_0)$ . The reflection coefficient  $r_0$  and the vector  $\mathbf{g}_0$  satisfy the following four-by-four linear system, derived from the boundary condition (9) at the top edge of the plate:

$$\mathbb{K} \mathcal{N}_{\text{down}}(H) \mathbf{g}_0 - r_0 \mathbf{h}_{\text{up}} = \mathbf{h}_{\text{down}}. \quad (14)$$

### 2.2.3 Reflection matrices and transmission vectors

Then the first downgoing wave in the plate arrives to the lower interface and gives an upgoing reflected elastodynamic wave and a downgoing transmitted acoustic wave (see Fig. 2) characterized by the following coefficients:

$$\mathbf{g}_1 = \mathcal{R}_{\text{bot}} \mathbf{g}_0 \quad \text{and} \quad t_1 = \mathbf{t}_{\text{bot}}^T \mathbf{g}_0, \quad (15)$$

the superscript  $\text{T}$  denoting transposition, the three-by-three reflection matrix  $\mathcal{R}_{\text{bot}}$  and the three-dimensional transmission vector  $\mathbf{t}_{\text{bot}}$  satisfying the following equation derived from the boundary condition (10) at the bottom edge of the plate:

$$\mathbb{K} \mathcal{N}_{\text{up}}(-H) \mathcal{R}_{\text{bot}} - \mathbf{h}_{\text{down}} \mathbf{t}_{\text{bot}}^{\text{T}} = -\mathbb{K} \mathcal{N}_{\text{down}}(-H) . \quad (16)$$

Similarly, the first reflected wave in the plate reaches the upper interface and generates a second reflected elastodynamic wave and an upgoing transmitted acoustic wave characterized by the following coefficients:

$$\mathbf{g}_2 = \mathcal{R}_{\text{top}} \mathbf{g}_1 \quad \text{and} \quad r_2 = \mathbf{t}_{\text{top}}^{\text{T}} \mathbf{g}_1 , \quad (17)$$

the reflection matrix  $\mathcal{R}_{\text{top}}$  and the transmission vector  $\mathbf{t}_{\text{top}}$  satisfying the following equation derived from the boundary condition (9):

$$\mathbb{K} \mathcal{N}_{\text{down}}(H) \mathcal{R}_{\text{top}} - \mathbf{h}_{\text{up}} \mathbf{t}_{\text{top}}^{\text{T}} = -\mathbb{K} \mathcal{N}_{\text{up}}(H) , \quad (18)$$

and so on, until infinity.

Hence, each  $2n^{\text{th}}$  reflected elastodynamic wave is downgoing,  $\mathbf{U}_{2n}(z) = a_{\text{inc}} \mathcal{N}_{\text{down}}(z) \mathbf{g}_{2n}$ , and brings about a downgoing acoustic wave below the plate:

$$p_{2n+1}(z) = a_{\text{inc}} \sqrt{\frac{2s_z}{\rho}} \exp[i s_z (z + H)] t_{2n+1} , \quad \text{where} \quad t_{2n+1} = \mathbf{t}_{\text{bot}}^{\text{T}} \mathbf{g}_{2n} . \quad (19)$$

Each  $(2n-1)^{\text{th}}$  reflected elastodynamic wave is upgoing,  $\mathbf{U}_{2n-1}(z) = a_{\text{inc}} \mathcal{N}_{\text{up}}(z) \mathbf{g}_{2n-1}$ , and produces an upgoing acoustic wave above the plate:

$$p_{2n}(z) = a_{\text{inc}} \sqrt{\frac{2s_z}{\rho}} \exp[-i s_z (z - H)] r_{2n} , \quad \text{where} \quad r_{2n} = \mathbf{t}_{\text{top}}^{\text{T}} \mathbf{g}_{2n-1} . \quad (20)$$

Successive values of the vector  $\mathbf{g}_N$  are derived from the recurrence properties:

$$\mathbf{g}_{2n} = \mathcal{R}_{\text{top}} \mathbf{g}_{2n-1} \quad \text{and} \quad \mathbf{g}_{2n+1} = \mathcal{R}_{\text{bot}} \mathbf{g}_{2n} , \quad (21)$$

as follows:

$$\mathbf{g}_{2n} = (\mathcal{R}_{\text{top}} \mathcal{R}_{\text{bot}})^n \mathbf{g}_0 \quad \text{and} \quad \mathbf{g}_{2n+1} = \mathcal{R}_{\text{bot}} (\mathcal{R}_{\text{top}} \mathcal{R}_{\text{bot}})^n \mathbf{g}_0 . \quad (22)$$

## 2.2.4 Global transfer functions

The state vector  $\mathbf{U}(z)$  characterizing the vibration of the plate is the sum of all the upgoing and downgoing waves:

$$\mathbf{U}(z) = a_{\text{inc}} [\mathcal{N}_{\text{up}}(z) \mathbf{g}_{\text{up}} + \mathcal{N}_{\text{down}}(z) \mathbf{g}_{\text{down}}] , \quad (23)$$

where the global transfer vectors  $\mathbf{g}_{\text{down}}$  and  $\mathbf{g}_{\text{up}}$  are obtained by using the so-called Debye series:

$$\mathbf{g}_{\text{down}} = \sum_{n=0}^{\infty} \mathbf{g}_{2n} = \left[ \sum_{n=0}^{+\infty} (\mathcal{R}_{\text{top}} \mathcal{R}_{\text{bot}})^n \right] \mathbf{g}_0 , \quad (24)$$

and

$$\mathbf{g}_{\text{up}} = \sum_{n=0}^{\infty} \mathbf{g}_{2n+1} = \mathcal{R}_{\text{bot}} \left[ \sum_{n=0}^{+\infty} (\mathcal{R}_{\text{top}} \mathcal{R}_{\text{bot}})^n \right] \mathbf{g}_0 = \mathcal{R}_{\text{bot}} \mathbf{g}_{\text{down}} . \quad (25)$$

The reflection coefficient  $r$  and the transmission coefficient  $t$  defined by Eq. (12) are derived from Eqs. (14–25):

$$r = r_0 + \sum_{n=0}^{+\infty} r_{2n+2} = r_0 + \mathbf{t}_{\text{top}}^{\text{T}} \left\{ \mathcal{R}_{\text{bot}} \left[ \sum_{n=0}^{+\infty} (\mathcal{R}_{\text{top}} \mathcal{R}_{\text{bot}})^n \right] \mathbf{g}_0 \right\} = r_0 + \mathbf{t}_{\text{top}}^{\text{T}} \mathbf{g}_{\text{up}} , \quad (26)$$

and

$$t = \sum_{n=0}^{+\infty} t_{2n+1} = \mathbf{t}_{\text{bot}}^{\text{T}} \left\{ \left[ \sum_{n=0}^{+\infty} (\mathcal{R}_{\text{top}} \mathcal{R}_{\text{bot}})^n \right] \mathbf{g}_0 \right\} = \mathbf{t}_{\text{bot}}^{\text{T}} \mathbf{g}_{\text{down}} . \quad (27)$$

The boundary conditions (9) and (10) are rewritten with respect to the global transfer functions by using Eqs. (12) and (23) at the upper interface:

$$\mathbb{K} [\mathcal{N}_{\text{up}}(H) \mathbf{g}_{\text{up}} + \mathcal{N}_{\text{down}}(H) \mathbf{g}_{\text{down}}] = \mathbf{h}_{\text{down}} + r \mathbf{h}_{\text{up}} , \quad (28)$$

and at the lower interface:

$$\mathbb{K} [\mathcal{N}_{\text{up}}(-H) \mathbf{g}_{\text{up}} + \mathcal{N}_{\text{down}}(-H) \mathbf{g}_{\text{down}}] = t \mathbf{h}_{\text{down}} . \quad (29)$$

Because combining Eqs. (24) and (25) leads to  $\mathbf{g}_{\text{down}} = \mathbf{g}_0 + \mathcal{R}_{\text{top}} \mathbf{g}_{\text{up}}$ , it is obvious from Eqs. (14), (16), (18) and (24–27) that the boundary conditions (28) and (29) are satisfied.

### 2.2.5 Debye series

The sum of the series contained in Eqs. (24)–(27) can be analytically obtained under the following condition:

$$\lambda_{\text{max}} \leq 1 , \quad (30)$$

where  $\lambda_{\text{max}}$  denotes the maximum of the absolute values of the eigenvalues of the matrix  $(\mathcal{R}_{\text{top}} \mathcal{R}_{\text{bot}})$ .

Thus, the sum of this geometrical series is immediately expressed by:

$$\sum_{n=0}^{+\infty} (\mathcal{R}_{\text{top}} \mathcal{R}_{\text{bot}})^n = (\mathbb{I}_3 - \mathcal{R}_{\text{top}} \mathcal{R}_{\text{bot}})^{-1} , \quad (31)$$

$\mathbb{I}_k$  denoting the  $k$ -by- $k$  identity matrix. The validity of this algebraic transformation seems to be natural from a physicist's point of view, since this equation results from summing multiple reflections/refractions in the framework of linear acoustics.

As a natural consequence, one can believe that the Debye series necessarily converges. Paradoxically, this is wrong for some angles of incidence and frequencies. Indeed, in the case of ultrasonic propagation in a submerged isotropic plate, it has been observed [8][7] that the Debye series expansion can diverge if the incidence angle is greater than the first critical angle. In accordance with literature, for an aluminum plate immersed in water, a convergence study will be summarized in Section 4.

The explanation of this unexpected divergence can be found by the analysis of energy fluxes. This analysis is made below for an anisotropic elastic material and leads to an alternative Debye series which necessarily converges.

Before closing this section, it should be noted that, beyond the physical aspect, all the equations previously obtained hold true whatever the definition of the upgoing and downgoing waves is, until the reflection and refraction terms  $\mathbf{g}_0$ ,  $r_0$ ,  $\mathcal{R}_{\text{bot}}$ ,  $\mathbf{t}_{\text{bot}}$ ,  $\mathcal{R}_{\text{top}}$  and  $\mathbf{t}_{\text{top}}$  ensure the boundary conditions at each interface. This is why the acoustic fields  $\mathbf{U}_{\text{up}}(z)$  and  $\mathbf{U}_{\text{down}}(z)$  have not been detailed above in Eq. (13). They will be expressed by two different ways in the next section.

### 3 Energy considerations on upgoing and downgoing waves in the plate

#### 3.1 Non orthogonality of the exponential solution basis in the sense of energy

##### 3.1.1 Normalization of the usual exponential solution basis, upgoing and downgoing waves

Let us now detail the classical analysis.

The following alternative formulation of Eq. (5) recalls that the state-vector  $\mathbf{U}(z)$  is the sum of six exponential components:

$$\mathbf{U}(z) = \sum_{\alpha=1}^6 a_{\alpha} \exp(-i \varsigma_{\alpha} z) \boldsymbol{\xi}_{\alpha}. \quad (32)$$

The six pairs (slowness  $\varsigma_{\alpha}$ , polarization vector  $\boldsymbol{\xi}_{\alpha}$ ) are defined above [Eq. (6)]. (2r) of them are real and correspond to homogeneous (or bulk) waves. (3 - r) pairs of them are complex conjugate and define *conjugate* inhomogeneous (or surface) waves.

Note that the number r of upgoing (or downgoing) homogeneous waves only depends on the incidence angle  $\theta$ . Before the first critical angle of incidence, the six components corresponds to bulk waves (r = 3). Beyond this critical angle, there is at least one pair of conjugate inhomogeneous waves (r ≤ 2, e.g., [17]).

Furthermore, the polarizations can be arbitrarily normalized by using the fact that the matrix ( $\boldsymbol{\Xi}^T \mathbb{T} \boldsymbol{\Xi}$ ) is diagonal (orthogonality relation slightly different from [11]), that is:

$$\forall \alpha, \beta; \alpha \neq \beta \implies \boldsymbol{\xi}_{\alpha}^T \mathbb{T} \boldsymbol{\xi}_{\beta} = 0, \quad \text{where } \mathbb{T} = \frac{-1}{4} \begin{pmatrix} \mathbb{O} & \mathbb{I}_3 \\ \mathbb{I}_3 & \mathbb{O} \end{pmatrix}, \quad (33)$$

$\mathbb{O}$  denoting the zero matrix of any dimension.

The matrix  $\mathbb{T}$  is taken such that  $\boldsymbol{\xi}_{\alpha}^T \mathbb{T} \boldsymbol{\xi}_{\alpha}$  is the third component of the Poynting vector of the  $\alpha^{\text{th}}$  exponential solution if both the  $z$ -component of the slowness and the polarization vectors are real-valued, i.e.  $\boldsymbol{\xi}_{\alpha}^T \mathbb{T} \boldsymbol{\xi}_{\alpha}$  is the average power flux in the  $z$ -direction for any homogeneous solution. That is the reason why both the matrix  $\mathbb{T}$  and the normalization of the polarization vectors [Eq. (38) below] are different from the literature.

Indeed, the slowness vector  $\mathbf{s}_{\alpha}$  of the  $\alpha^{\text{th}}$  exponential solution being  $\begin{bmatrix} s_x & 0 & \varsigma_{\alpha} \end{bmatrix}^T$ , the velocity vector being  $\mathbf{v}_{\alpha}(z) = \exp(-i \omega \varsigma_{\alpha} z) \mathbf{v}_{\alpha}$ , where  $\varsigma_{\alpha} = \varsigma'_{\alpha} - i \varsigma''_{\alpha}$ , and the Hooke's law giving the stress  $\boldsymbol{\Sigma}_{\alpha}$  in any direction defined by the unit vector  $\mathbf{d}$  as follows:

$$\boldsymbol{\Sigma}_{\alpha}(z) \mathbf{d} = -(\mathbf{d} \diamond \mathbf{s}_{\alpha}) \mathbf{v}_{\alpha}(z) = -\exp(-i \omega \varsigma_{\alpha} z) (\mathbf{d} \diamond \mathbf{s}_{\alpha}) \mathbf{v}_{\alpha}, \quad (34)$$

by using the properties (8) of the diamond product, we obtain the Poynting vector  $\mathbf{p}_{\alpha}$  in the general case:

$$\mathbf{p}_{\alpha}(z) = \frac{-1}{4} [\boldsymbol{\Sigma}_{\alpha}^*(z) \mathbf{v}_{\alpha}(z) + \boldsymbol{\Sigma}_{\alpha}(z) \mathbf{v}_{\alpha}^*(z)] = \frac{1}{4} \exp(-2 \omega \varsigma''_{\alpha} z) [(\mathbf{v}_{\alpha}^* \diamond \mathbf{v}_{\alpha}) \mathbf{s}_{\alpha} + (\mathbf{v}_{\alpha} \diamond \mathbf{v}_{\alpha}^*) \mathbf{s}_{\alpha}^*]. \quad (35)$$

The average power flux  $\phi_{\alpha}$  in the  $z$ -direction is immediately deduced by  $\phi_{\alpha}(z) = \mathbf{n}^T \mathbf{p}_{\alpha}(z)$ . Together with Eqs. (34) and (35), it implies that the polarization vector of the stress in the  $z$ -direction satisfies  $\boldsymbol{\tau}_{\alpha} = -(\mathbf{n} \diamond \mathbf{s}_{\alpha}) \mathbf{v}_{\alpha}$ , and that:

$$\boldsymbol{\xi}_{\alpha}^T \mathbb{T} \boldsymbol{\xi}_{\alpha} = \frac{-1}{2} \mathbf{v}_{\alpha}^T \boldsymbol{\tau}_{\alpha} = \frac{1}{2} \mathbf{n}^T (\mathbf{v}_{\alpha} \diamond \mathbf{v}_{\alpha}) \mathbf{s}_{\alpha}, \quad (36)$$

is the average power flux in the  $z$ -direction for homogeneous solutions only ( $\varsigma''_{\alpha} = 0$  and real-valued polarization). This flux  $\phi_{\alpha}$  is independent from the position  $z$  (energy conservation). On the contrary,  $\boldsymbol{\xi}_{\alpha}^T \mathbb{T} \boldsymbol{\xi}_{\alpha}$  does not

correspond to a power flux for inhomogeneous solutions but it is nevertheless used for normalization (38), as done in the literature.

Note that the orthogonality relation (33) can be also rewritten as follows:

$$\forall \alpha, \beta; \alpha \neq \beta \implies \mathbf{n}^T [(\mathbf{v}_\beta \diamond \mathbf{v}_\alpha) \mathbf{s}_\alpha + (\mathbf{v}_\alpha \diamond \mathbf{v}_\beta) \mathbf{s}_\beta] = 0. \quad (37)$$

Assuming for simplicity that the six eigenvalues are different, the following convention is used to include the sign of the energy fluxes in the  $z$ -direction, instead of the normalization encountered in the literature (see *e.g.* [19, Eq. (42)], [12], [13], [17, Eq. (56)]):

$$\begin{aligned} \varsigma_\alpha \in \mathbb{R} & \quad , \quad \boldsymbol{\xi}_\alpha \in \mathbb{R}^6 & \quad , \quad \boldsymbol{\xi}_\alpha^T \mathbb{T} \boldsymbol{\xi}_\alpha = \phi_\alpha = 1 & \quad , \quad 1 \leq \alpha \leq r & \quad , \\ \mathcal{I}m(\varsigma_\alpha) < 0 & \quad , \quad \mathcal{I}m(\boldsymbol{\xi}_\alpha) \neq \mathbf{0}_6 & \quad , \quad \boldsymbol{\xi}_\alpha^T \mathbb{T} \boldsymbol{\xi}_\alpha = 1 & \quad , \quad r < \alpha \leq 3 & \quad , \\ \varsigma_\alpha \in \mathbb{R} & \quad , \quad \boldsymbol{\xi}_\alpha \in \mathbb{R}^6 & \quad , \quad \boldsymbol{\xi}_\alpha^T \mathbb{T} \boldsymbol{\xi}_\alpha = \phi_\alpha = -1 & \quad , \quad 4 \leq \alpha \leq 3+r & \quad , \\ \varsigma_\alpha = \varsigma_{\alpha-3}^* & \quad , \quad \boldsymbol{\xi}_\alpha = \boldsymbol{\xi}_{\alpha-3}^* & \quad , \quad \boldsymbol{\xi}_\alpha^T \mathbb{T} \boldsymbol{\xi}_\alpha = 1 & \quad , \quad 3+r < \alpha \leq 6 & \quad , \end{aligned} \quad (38)$$

such that the first three waves are upgoing (positive power flux  $\phi_\alpha$  for bulk waves/decreasing amplitude  $\exp(-\omega \varsigma_\alpha'' z)$  with increasing  $z$  for surface waves) and the last three waves are downgoing (negative power flux/decreasing amplitude with decreasing  $z$ ).

Consequently, the matrix  $\mathcal{N}(z) = \left[ \mathcal{N}_{\text{up}}(z) \middle| \mathcal{N}_{\text{down}}(z) \right]$  introduced in Eqs. (5) and (13) is now fully defined.

### 3.1.2 Study of orthogonality in the sense of energy

The  $z$ -component of the Poynting vector associated with the state-vector  $\mathbf{U}$  defines the mean power flux  $\phi$  through the plane  $z = z_0$ , which is independent from the position  $z_0$  as expected due to energy conservation. Combining the definition in Eq. (32) and the normalization convention given by Eq. (38) yields:

$$\phi = \mathbf{U}(z_0)^+ \mathbb{T} \mathbf{U}(z_0) = \mathbf{a}^+ \mathbb{J} \mathbf{a} = \sum_{\alpha=1}^r |a_\alpha|^2 - \sum_{\alpha=4}^{3+r} |a_\alpha|^2 + \sum_{\alpha=r+1}^3 a_\alpha a_{\alpha+3}^* + a_\alpha^* a_{\alpha+3}, \quad (39.a)$$

where the superscript  $+$  denotes the transposition combined with the complex conjugation. The non-diagonal Hermitian matrix  $\mathbb{J}$  is defined by:

$$\mathbb{J} = \mathcal{N}(z_0)^+ \mathbb{T} \mathcal{N}(z_0) = \boldsymbol{\Xi}^+ \mathbb{T} \boldsymbol{\Xi} = \begin{pmatrix} \mathbb{I}_r & \mathbb{O} & \mathbb{O} & \mathbb{O} \\ \mathbb{O} & \mathbb{O} & \mathbb{O} & \mathbb{I}_{3-r} \\ \mathbb{O} & \mathbb{O} & -\mathbb{I}_r & \mathbb{O} \\ \mathbb{O} & \mathbb{I}_{3-r} & \mathbb{O} & \mathbb{O} \end{pmatrix}. \quad (39.b)$$

Each upgoing homogeneous component  $a_\alpha$  ( $1 \leq \alpha \leq r$ ) contributes to the total power flux in the  $z$ -direction only by its own power flux  $|a_\alpha|^2$ , independently from the other components. The same holds for each downgoing homogeneous component whose contribution is  $-|a_\alpha|^2$  ( $4 \leq \alpha \leq 3+r$ ). A homogeneous component is orthogonal to any other one in the sense of energy.

On the contrary, it is obvious that the contribution of an inhomogeneous component depends also on its conjugate component: each component and its conjugate are orthogonal to themselves and to any other component but not to each other. Indeed if each inhomogeneous component is considered separately ( $a_\alpha \neq 0$  and  $a_{\alpha+3} = 0$ , or  $a_\alpha = 0$  and  $a_{\alpha+3} \neq 0$ ), its contribution to the total flux is zero, without any energy transfer along the  $z$ -direction. On the contrary, the conjunction of the two conjugate components, the coefficients  $a_\alpha$  and  $a_{\alpha+3}$  being both non-zero, can transfer energy along the  $z$ -direction.



such that the total power flux  $\phi$  in the  $z$ -direction [Eq. (40)] is the difference of the upgoing flux  $|\tilde{\mathbf{a}}_{\text{up}}|^2$  minus the downgoing flux  $|\tilde{\mathbf{a}}_{\text{down}}|^2$ .

Of course, by using this new definition of upgoing and downgoing waves, when they are inhomogeneous, all the associated reflection and refraction terms are different from those obtained by the usual way. They are calculated by reporting the expression (44) in the boundary equations (14), (16) and (18) and they are identified by a tilde to differentiate them:  $\tilde{\mathbf{g}}_0$ ,  $\tilde{r}_0$ ,  $\tilde{\mathcal{R}}_{\text{bot}}$ ,  $\tilde{\mathbf{t}}_{\text{bot}}$ ,  $\tilde{\mathcal{R}}_{\text{top}}$  and  $\tilde{\mathbf{t}}_{\text{top}}$ .

The non-uniqueness of this basis has to be pointed out. Indeed, for each set of  $z_\alpha$  values, a different basis is defined with upgoing and downgoing fluxes which can be modified although the total power flux in the  $z$ -direction remains equal to  $|\tilde{\mathbf{a}}_{\text{up}}|^2 - |\tilde{\mathbf{a}}_{\text{down}}|^2$ . To keep the symmetry of the problem, it seems natural that all the  $z_\alpha$  parameters are taken equal to zero. The choice of these parameters will be discussed for the isotropic case in the last section.

### 3.3 Spatial structure of the orthogonal waves

By separating real and imaginary parts of the slowness in the  $z$ -direction and of the polarization vector such that:

$$\varsigma_\alpha = \varsigma'_\alpha - \mathfrak{i} \varsigma''_\alpha \quad \text{and} \quad \boldsymbol{\xi}_\alpha = \boldsymbol{\xi}'_\alpha - \mathfrak{i} \boldsymbol{\xi}''_\alpha \quad (45)$$

and by including the implicit dependency on position  $x$  and time  $\tau$ , Equations (41) and (42) leads to the following expressions of the physical fields, with  $\delta z = z - z_\alpha$ :

$$\mathbf{V}_\alpha(x, z, \tau) = \mathcal{R}e \left\{ \sqrt{2} \exp[\mathfrak{i} \omega (\tau - s_x x - \varsigma'_\alpha \delta z)] \left[ \cosh(\omega \varsigma''_\alpha \delta z) \boldsymbol{\xi}'_\alpha + \mathfrak{i} \sinh(\omega \varsigma''_\alpha \delta z) \boldsymbol{\xi}''_\alpha \right] \right\} \quad (46)$$

for the upgoing wave, and:

$$\mathbf{V}_{\alpha+3}(x, z, \tau) = \mathcal{R}e \left\{ \sqrt{2} \exp[\mathfrak{i} \omega (\tau - s_x x - \varsigma'_\alpha \delta z)] \left[ \sinh(\omega \varsigma''_\alpha \delta z) \boldsymbol{\xi}'_\alpha + \mathfrak{i} \cosh(\omega \varsigma''_\alpha \delta z) \boldsymbol{\xi}''_\alpha \right] \right\}, \quad (47)$$

for the downgoing wave.

The latter equations show an elliptic polarization [22] except for  $\delta z = 0$  (linear polarization). The amplitude exponentially increases with the absolute value of  $\delta z$  since the mean power flux  $\phi$  along the  $z$ -direction remains equal to unity for the upgoing wave and to  $-1$  for the downgoing wave.

The wavefronts for the polarization component in the direction  $\mathbf{d}$  are defined by  $\mathbf{V}_{\alpha,\alpha+3}(x, z, \tau) \cdot \mathbf{d} = 0$  for any given time  $\tau$ . Note that the vector  $\mathbf{d}$  is six-dimensional and either its last three components or first three components are zero, such that to define a polarization direction of either velocity or stress, respectively. Thus, after some algebra we obtain the following equations of the wavefronts:

$$s_x (x - x_0) = -\varsigma'_\alpha \delta z + \frac{1}{\omega} \arctan \left[ \frac{\boldsymbol{\xi}''_\alpha \cdot \mathbf{d}}{\boldsymbol{\xi}'_\alpha \cdot \mathbf{d}} \tanh(\omega \varsigma''_\alpha \delta z) \right] \quad (48)$$

for the upgoing wave, the position  $x_0$  being any arbitrary value, and:

$$s_x (x - x_0) = -\varsigma'_\alpha \delta z - \frac{1}{\omega} \arctan \left[ \frac{\boldsymbol{\xi}'_\alpha \cdot \mathbf{d}}{\boldsymbol{\xi}''_\alpha \cdot \mathbf{d}} \tanh(\omega \varsigma''_\alpha \delta z) \right] \quad (49)$$

for the downgoing wave.

In the case of an isotropic medium (see Appendix A), the real part  $\varsigma'_\alpha$  of the slowness in the  $z$ -direction is zero. The velocity field in the  $x$  direction for the upgoing  $P$  wave is obtained from Eqs. (46) and (A.10.a) and drawn in Fig 3. Eq. (48) simply becomes:  $\omega s_x (x - x_0) = -\arctan[\tanh(\delta \mathbb{Z})]$ , where  $\delta \mathbb{Z} = \omega \sqrt{s_x^2 - c_L^{-2}} \delta z$ . The

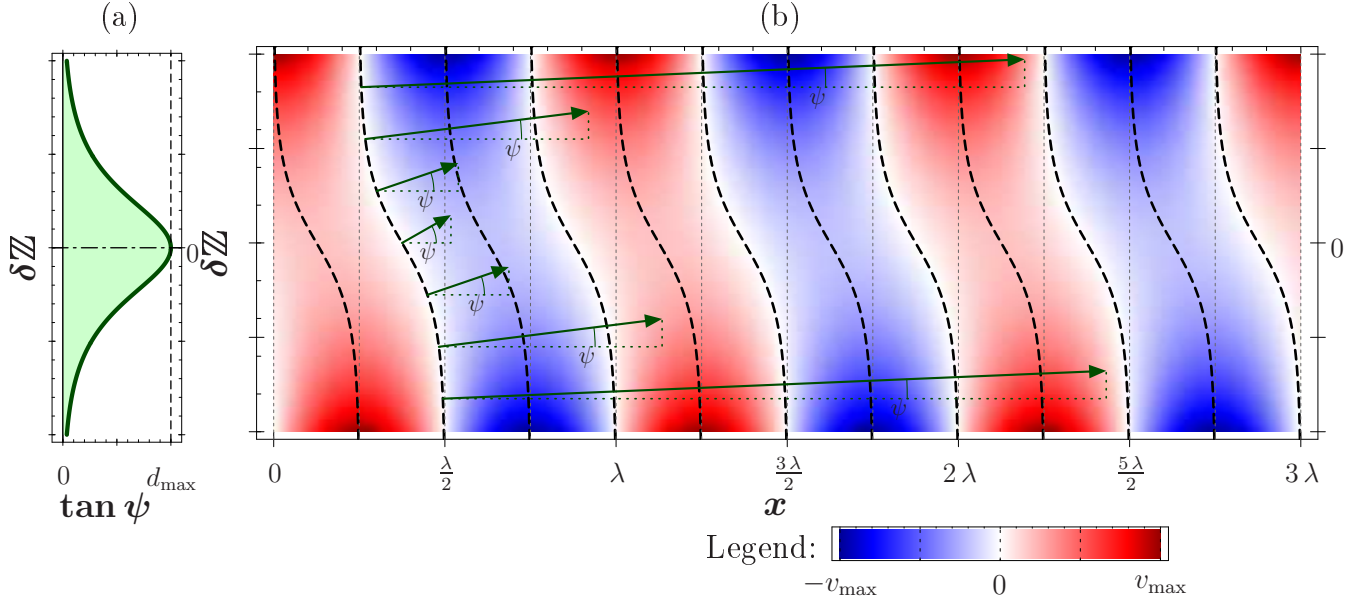


Figure 3: (b) Magnitude of non-zero coordinates of nonstandard progressive waves in isotropic elastic media. The dashed lines correspond to wavefronts. (a) Tangent of the angle  $\psi$  between the normal of the wavefronts and the  $x$ -axis:  $\tan \psi = d_{\max} / \cosh(2 \delta Z)$ .

tangent of the angle between the  $x$ -direction and the Poynting vector of the  $P$  wave [defined by Eq. (A.11)] is proportional to  $\cosh(2 \delta Z)^{-1}$ , as for the vectors normal to the wavefronts.

If we have a glance on the Poynting vectors  $\tilde{\mathbf{p}}_{\alpha, \alpha+3}$  of the upgoing/downgoing orthogonal waves, the velocity vector being:

$$\tilde{\mathbf{v}}_{\alpha, \alpha+3}(z) = \frac{1}{\sqrt{2}} \exp(-i \omega \zeta'_\alpha \delta z) [ \pm \exp(-\omega \zeta''_\alpha \delta z) \mathbf{v}_\alpha + \exp(\omega \zeta''_\alpha \delta z) \mathbf{v}_\alpha^* ] \quad (50)$$

and the stress tensor in any direction  $\mathbf{l}$  being defined by:

$$\tilde{\Sigma}_{\alpha, \alpha+3}(z) \mathbf{l} = \frac{-1}{\sqrt{2}} \exp(-i \omega \zeta'_\alpha \delta z) [ \pm \exp(-\omega \zeta''_\alpha \delta z) (\mathbf{l} \diamond \mathbf{s}_\alpha) \mathbf{v}_\alpha + \exp(\omega \zeta''_\alpha \delta z) (\mathbf{l} \diamond \mathbf{s}_\alpha^*) \mathbf{v}_\alpha^* ], \quad (51)$$

these Poynting vectors are expressed as follows:

$$\tilde{\mathbf{p}}_{\alpha, \alpha+3}(z) = \tilde{\mathbf{j}}_{\alpha s}(\delta z) \pm \tilde{\mathbf{j}}_{\alpha I}, \quad (52.a)$$

where

$$\tilde{\mathbf{j}}_{\alpha s}(\delta z) = \frac{1}{4} \cosh(2 \omega \zeta''_\alpha \delta z) [ (\mathbf{v}_\alpha^* \diamond \mathbf{v}_\alpha) \mathbf{s}_\alpha + (\mathbf{v}_\alpha \diamond \mathbf{v}_\alpha^*) \mathbf{s}_\alpha^* ], \quad (52.b)$$

is proportional to the sum of the Poynting vectors of the conjugate inhomogeneous waves [Eq. (35)], and

$$\tilde{\mathbf{j}}_{\alpha I} = \frac{1}{4} [ (\mathbf{v}_\alpha \diamond \mathbf{v}_\alpha) \mathbf{s}_\alpha + (\mathbf{v}_\alpha^* \diamond \mathbf{v}_\alpha^*) \mathbf{s}_\alpha^* ], \quad (52.c)$$

represents the interaction between the conjugate inhomogeneous waves.

From Eqs. (35), (38), (52) and the orthogonality relation (37), it is obvious that  $\mathbf{n}^T \tilde{\mathbf{j}}_{\alpha s}(\delta z) = 0$  and  $\mathbf{n}^T \tilde{\mathbf{j}}_{\alpha I} = 1$ , *i.e.* the vector  $\tilde{\mathbf{j}}_{\alpha s}$  is in the  $xy$  plane whereas the third component of the vector  $\tilde{\mathbf{j}}_{\alpha I}$  is normalized by construction.

For an isotropic material, the uniform flux  $\tilde{\mathbf{j}}_{\alpha I}$  is vertical (in the  $z$ -direction) and the horizontal flux  $\tilde{\mathbf{j}}_{\alpha s}(\delta z)$  is in the  $x$ -direction and proportional to  $\cosh(2 \omega \zeta''_\alpha \delta z)$  (see Appendix A).

### 3.4 Relations between the energy fluxes in the $z$ -direction

Through the energy conservation equations, some reflection and refraction coefficients are related between them. These equations depend on the interface investigated and on the definition of upgoing and downgoing waves.

For the reflection/refraction of the incident wave at the upper interface, in the standard exponential basis, only the  $r$  homogeneous waves transmit energy in the  $z$ -direction as shown by the following conservation equation:

$$|r_0|^2 + \sum_{\alpha=1}^r |g_{0,\alpha}|^2 = 1. \quad (53)$$

As demonstrated above [Eq. (39)], the amplitudes  $(g_{0,\alpha})_{r < \alpha \leq 3}$  of the inhomogeneous waves are not included in the latter equation.

On the contrary, in the orthogonal basis, it is obvious that each downgoing wave transmit energy, which leads to:

$$|\tilde{r}_0|^2 + |\tilde{\mathbf{g}}_0|^2 = 1. \quad (54)$$

Same types of relations are obtained when studying the reflections at each interface. In the standard exponential basis, the energy conservation can involve interaction fluxes if inhomogeneous waves exist, *i.e.* above the first critical angle. The energy relations are written as follows:

$$\sum_{\alpha=1}^r |\mathbf{g}_{2n,\alpha}|^2 = \sum_{\alpha=1}^r |\mathbf{g}_{2n+1,\alpha}|^2 + \sum_{\alpha=r+1}^3 (\mathbf{g}_{2n,\alpha} \mathbf{g}_{2n+1,\alpha}^* + \mathbf{g}_{2n+1,\alpha}^* \mathbf{g}_{2n,\alpha}) + |t_{2n+1}|^2, \quad (55)$$

at the lower interface, and:

$$\sum_{\alpha=1}^r |\mathbf{g}_{2n+1,\alpha}|^2 = \sum_{\alpha=1}^r |\mathbf{g}_{2n+2,\alpha}|^2 - \sum_{\alpha=r+1}^3 (\mathbf{g}_{2n+1,\alpha} \mathbf{g}_{2n+2,\alpha}^* + \mathbf{g}_{2n+2,\alpha}^* \mathbf{g}_{2n+1,\alpha}) + |r_{2n+2}|^2, \quad (56)$$

at the upper interface.

In the orthogonal basis, the energy conservation is simply written as follows:

$$|\tilde{\mathbf{g}}_{2n}|^2 = |\tilde{\mathbf{g}}_{2n+1}|^2 + |\tilde{t}_{2n+1}|^2, \quad |\tilde{\mathbf{g}}_{2n+1}|^2 = |\tilde{\mathbf{g}}_{2n+2}|^2 + |\tilde{r}_{2n+2}|^2, \quad (57)$$

at lower and upper interfaces, respectively. Hence, by combining Eqs. (19), (20), (21) and (57), the following equation of conservation is found:

$$|\tilde{\mathbf{r}}_\alpha|^2 + |\tilde{t}_\alpha|^2 = 1, \quad (58)$$

which relates each column-vector  $\tilde{\mathbf{r}}_\alpha$  of the matrix  $\tilde{\mathcal{R}}_{\text{top,bot}}$  and each component  $\tilde{t}_\alpha$  of the vector  $\tilde{\mathbf{t}}_{\text{top,bot}}$ .

This is the key point to guarantee the Debye series convergence. As a matter of fact, from the latter equation, it is made clear that the absolute values of the eigenvalues of the product  $\tilde{\mathcal{R}}_{\text{top}} \tilde{\mathcal{R}}_{\text{bot}}$  are necessarily less or equal than one, because the matrices  $\tilde{\mathcal{R}}_{\text{top}}$  and  $\tilde{\mathcal{R}}_{\text{bot}}$  are one-lipschitzian matrices, *i.e.*  $|\tilde{\mathcal{R}}_{\text{top,bot}} \mathbf{u}| \leq |\mathbf{u}|$  for any vector  $\mathbf{u}$ .

## 4 Numerical results for an aluminum plate immersed in water

To fix ideas, numerical results are reported and discussed in this section. Even though the theoretical results obtained in the last sections are valuable for any anisotropies and any planes of incidence, this analysis is restricted for simplicity to the concrete example of an aluminum plate immersed in water, for which the parameter values and some physical quantities are given in Table 1.

(a)				
Aluminum			Water	
Density	Longitudinal velocity	Transverse velocity	Density	Sound velocity
$\rho_0 = 2700 \text{ kg}\cdot\text{m}^{-3}$	$c_L = 6420 \text{ m}\cdot\text{s}^{-1}$	$c_T = 3040 \text{ m}\cdot\text{s}^{-1}$	$\rho = 1000 \text{ kg}\cdot\text{m}^{-3}$	$c = 1550 \text{ m}\cdot\text{s}^{-1}$

(b)			
	Longitudinal	Transverse	Rayleigh
Adimensional slowness	$\frac{c_T}{c_L} \approx 0.474$	$\frac{c_T}{c} = 1$	$\frac{c_T}{c_R} \approx 1.069$
Critical angle: $\theta_x = \arcsin(c/c_x)$	$\theta_L \approx 13.97^\circ$	$\theta_T \approx 30.66^\circ$	$\theta_R \approx 33.01^\circ$

Table 1: Numerical values for aluminum and water: (a) velocities and densities; (b) dimensionless slownesses and critical angles.

### 4.1 Convergence study of the Debye Series

First of all, for inspection purpose, the convergence of the multiple reflection/refraction is analyzed for both the classical and the new approaches. To this end, for the classical solutions, in Fig. 4, the maximum  $\lambda_{\max}$  of the absolute values of eigenvalues, defined in Eq. (30), is plotted in a 3D graph versus the dimensionless half-thickness  $h$  ( $= \omega h / c_T$ ) and the angle of incidence  $\theta$ . In the darker areas the series diverges, *i.e.*  $\lambda_{\max} > 1$ , while in the lighter zones, it converges, *i.e.*  $\lambda_{\max} < 1$ . Indeed, the two critical angles  $\theta_L$  and  $\theta_T$  play a crucial role in the separation of convergence and divergence zones. The dispersion curves of Lamb waves, obtained for complex frequencies [23], are plotted also on Fig. 4, since these curves participate as well to the convergence area limits. It is remarkable to observe that the dispersion curves of the  $A_0$  and  $S_0$  modes separate very accurately two such zones. In addition, it is of interest to note that the intersection points between the line  $\theta = \theta_L$  and these dispersion curves define alternative zones of convergence or not.

Keeping in mind these observations, let us compare the global reflection and the sum of the series truncated at  $n = n_{\max}$ , for the given dimensionless half-thickness  $h = 2$ . Figures 5-a and 5-b present these coefficients as a function of the angle of incidence  $\theta$ , for the classical approach and the solution proposed in this paper, respectively, and for various  $n_{\max} = 0, 2$  and  $10$ . Obviously, for angles of incidence less than the first critical angle  $\theta_L$ , both results are identical, since not any inhomogeneous wave is involved in the reflection/refraction process. Differences appear just after this angle (or after  $\theta_T$ ). The divergence of the series is visible in Figure 5-a for the classical solution, between this angle (or  $\theta_T$ ) and  $\theta_1$  (or  $\theta_2$ ), in agreement with the convergence study presented in Fig. 4. In contrast, for the new series, the convergence is ensured for all angles of incidence. However, by analyzing the behavior when  $n_{\max}$  increases on Fig. 5-b, it should be observed that this convergence is relatively slow.

As has been pointed out in the previous section, the choice of the dimensionless origins  $z_{\text{sv}} = \omega z_{\text{sv}} / c_T$  and  $z_{\text{p}} = \omega z_{\text{p}} / c_T$  is arbitrary [*cf.* Eqs. (41–42) and Appendix A.2]. These origins can be different for each partial wave. In addition, this choice influences the rapidity of the series convergence, while convergence is ensured for any values of the parameters  $z_{\text{sv}}$  and  $z_{\text{p}}$ . For this reason, the latter comments on Fig. 5-b are relative to this choice *i.e.* corresponds to  $z_{\text{sv}} = z_{\text{p}} = 0$  in that case. From that point of view, it can even be possible that

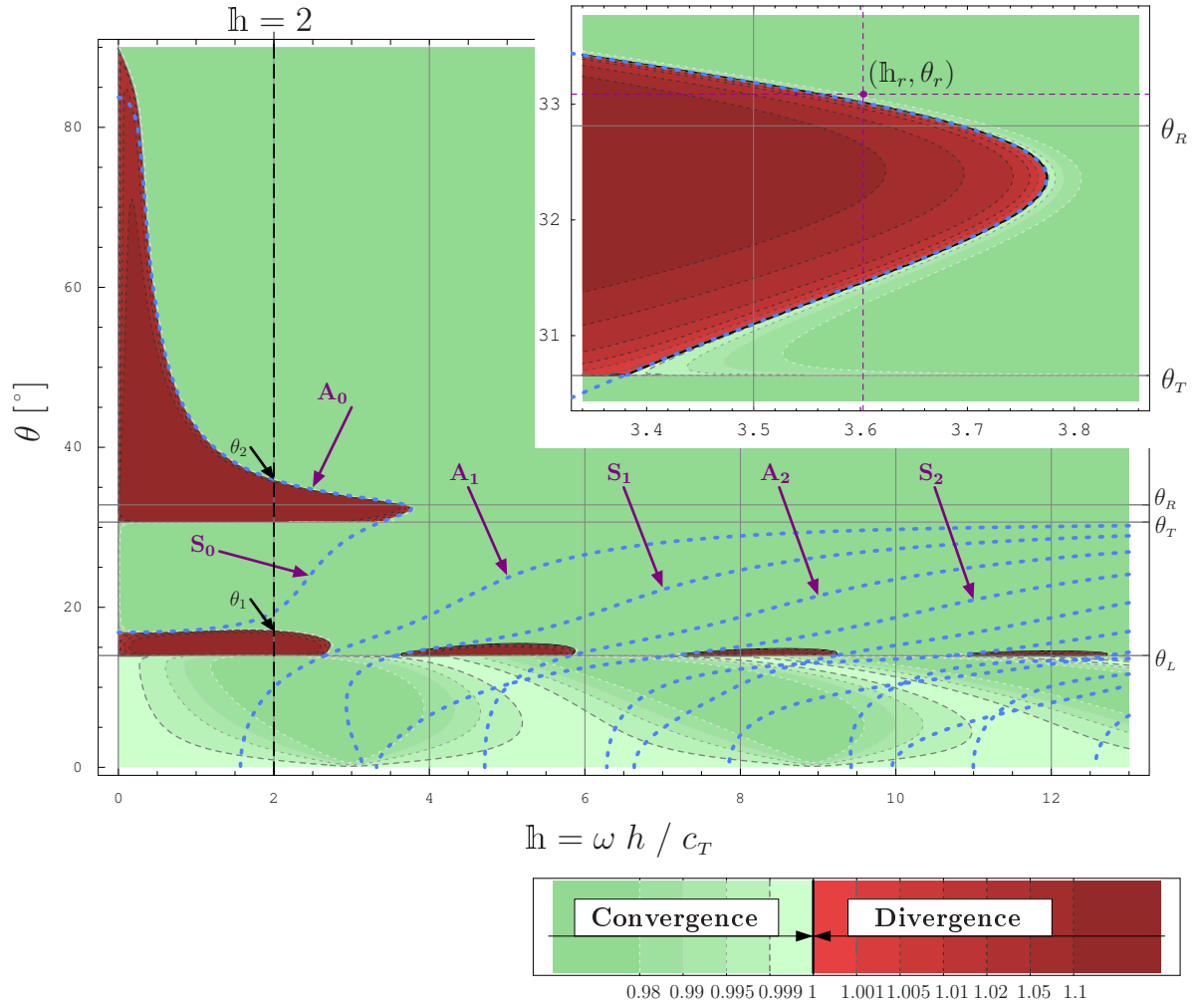


Figure 4: Study of the convergence of Debye series for an aluminum plate immersed in water. Maximum  $\lambda_{\max}$  of the absolute values of eigenvalues of the  $(\mathcal{R}_{\text{top}} \mathcal{R}_{\text{bot}})$  matrix versus the dimensionless frequency-half-thickness product  $\mathfrak{h} = \omega h / c_T$  and the incidence angle  $\theta$ . Only  $P$  and  $SV$  waves are considered. The light zone corresponds to the convergence ( $\lambda_{\max} < 1$ ) and the dark zone to the divergence ( $\lambda_{\max} > 1$ ).

the series converges either rapidly or slowly for the same configuration (fluid, solid, plate thickness and angle of incidence). To illustrate our purpose, Fig. 6 shows, for various  $z_{\text{SV}}$  and  $z_{\text{P}}$ , the maximum  $\tilde{\lambda}_{\max}$  of the absolute values of the eigenvalues of the matrix  $(\tilde{\mathcal{R}}_{\text{top}} \tilde{\mathcal{R}}_{\text{bot}})$ , which characterizes the series convergence [see Eqs. (30-31)]. On this 3D plot, the dark and light areas correspond to rapid and slow convergences, respectively. For the angle of incidence chosen ( $\theta=34.0^\circ$ ), if both origins are at the symmetry center of the plate (*i.e.*  $z_{\text{SV}}=z_{\text{P}}=0$ ), the convergence is in between these two extreme cases, as observed on Fig. 5-b.

## 4.2 The first reflection/refraction at the upper interface

Another consequence of the arbitrary choice of the  $z$ -origins concerns the reflection and the transmission at the first interface. The associated coefficients, *i.e.*  $\tilde{r}_0$ ,  $\tilde{g}_{0\text{SV}}$  and  $\tilde{g}_{0\text{P}}$ , do not affect directly the convergence of the series but they provide the input power flux in the plate, this latter flux being then spread out between the different reflections and transmissions at the two interfaces.

Let us inspect first the behavior of these coefficients for the classical case (see Fig. 7-a). As well known, for such plate, *i.e.* when the slower wave speed for bulk waves in the plate is greater than the fluid wave speed, the reflection coefficient  $r_0$  has an absolute value equal to unity after the larger critical angle and, at the same time, the modulus of the transmission coefficients  $g_{0\text{SV}}$  and  $g_{0\text{P}}$  are greater than unity. This is not at all in

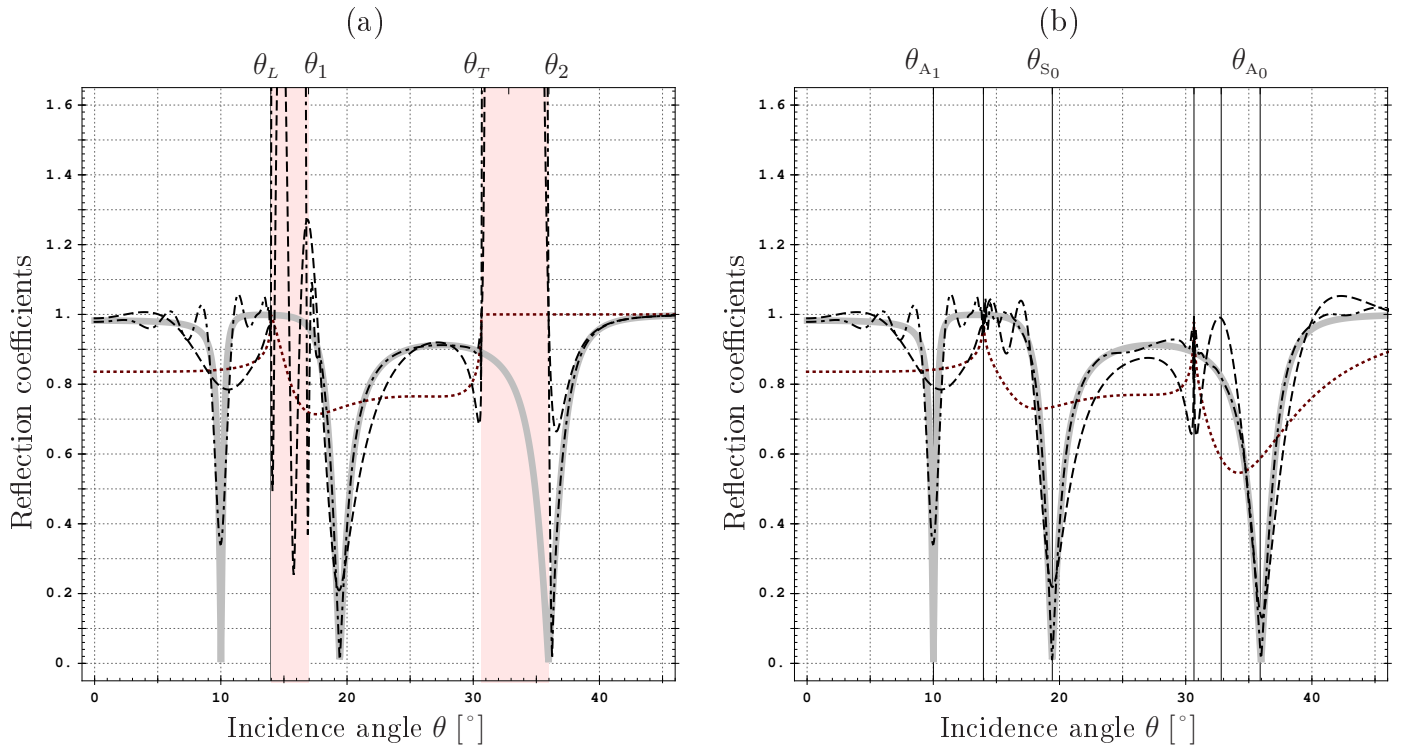


Figure 5: Convergence study for a dimensionless half-thickness  $h = \omega h / c_T = 2$  (a) in the exponential basis and (b) in the orthogonal symmetric basis ( $z_\alpha=0$  for all  $\alpha$ ). The absolute value of the global reflection coefficient  $|r|$  (plain) is compared to  $\left| \sum_{n=0}^{n_{\max}} r_{2n} \right|$  for  $n_{\max}=0$  (first reflection, dotted),  $n_{\max}=2$  (dashed) and  $n_{\max}=10$  (—).

contradiction with the energy conservation law, since the associated relation, Eq. (53) in this case, does not involve the inhomogeneous waves. The amplitude of such waves is *a priori* not bounded. In contrast, when all the wave amplitudes are connected by Eq. (53), *i.e.*  $\theta < \theta_L$ , all coefficients have absolute value less than unity.

By using the wave decomposition in the orthogonal basis, the reflection and refraction coefficients remain unchanged for each fixed pair  $(\delta h_{SV}, \delta h_P)$ ,  $\delta h_{SV,P} = \omega(h - z_{SV,P}) / c_T$  being the dimensionless relative positions of the upper interface with respect to the  $z$ -origins of the nonstandard SV- and P-waves, respectively (see also Appendix A.3 for more details). These reflection and refraction coefficients are plotted on Fig. 7-b to Fig. 7-d for three different pairs. Indeed, by virtue of Eq. (54), it is observed that the coefficients  $\tilde{g}_{0SV}$  and  $\tilde{g}_{0P}$  have absolute value less than unity for any angles of incidence. Of course, all these coefficients are different from those of the classical approach after the critical angle  $\theta_L$ , since the inhomogeneous waves are differently defined. For instance, the absolute value of the reflection coefficient  $\tilde{r}_0$  is not equal to unity and the reflection coefficients  $\tilde{g}_{0SV}$  and  $\tilde{g}_{0P}$  are nonzero, for  $\theta > \theta_T$ , although these coefficients are relative to the first interface only. Since the square of the absolute values of all the reflection or refraction coefficients give directly the reflected or refracted energy fluxes in the  $z$ -direction, this means that some energy is transmitted inside the plate, even for such angle of incidence.

Taking into account the dependence of the reflection and refraction coefficients on the pair  $(\delta h_{SV}, \delta h_P)$  naturally leads to the question: “*Is it possible to match the impedances at the first interface by conveniently choosing the  $z$ -origins  $z_{SV,P}$ ?*” The conditions of existence of such possibility are discussed theoretically in Appendix A.3 for the isotropic case and presented numerically on Fig. 8. For all the angles of incidence appearing in these figures in between two gray vertical zones, the reflection coefficient  $\tilde{r}_0$  is rigorously zero since the values of the dimensionless relative positions  $\delta h_{SV,P}$  have been chosen in accordance with Eq. (A.17). As predicted, around the Rayleigh conditions and close to the angle of incidence of  $90^\circ$ , the impedance can be totally matched such that the energy brought by the incident wave is totally transmitted inside the solid at the first interface. The values of the dimensionless relative positions are reported on Figs. 8-a and 8-b for the two inspected zones. The absolute value of the associated transmission coefficients  $g_{0SV}$  and  $g_{0P}$  are plotted on Figs. 8-c and 8-d. The

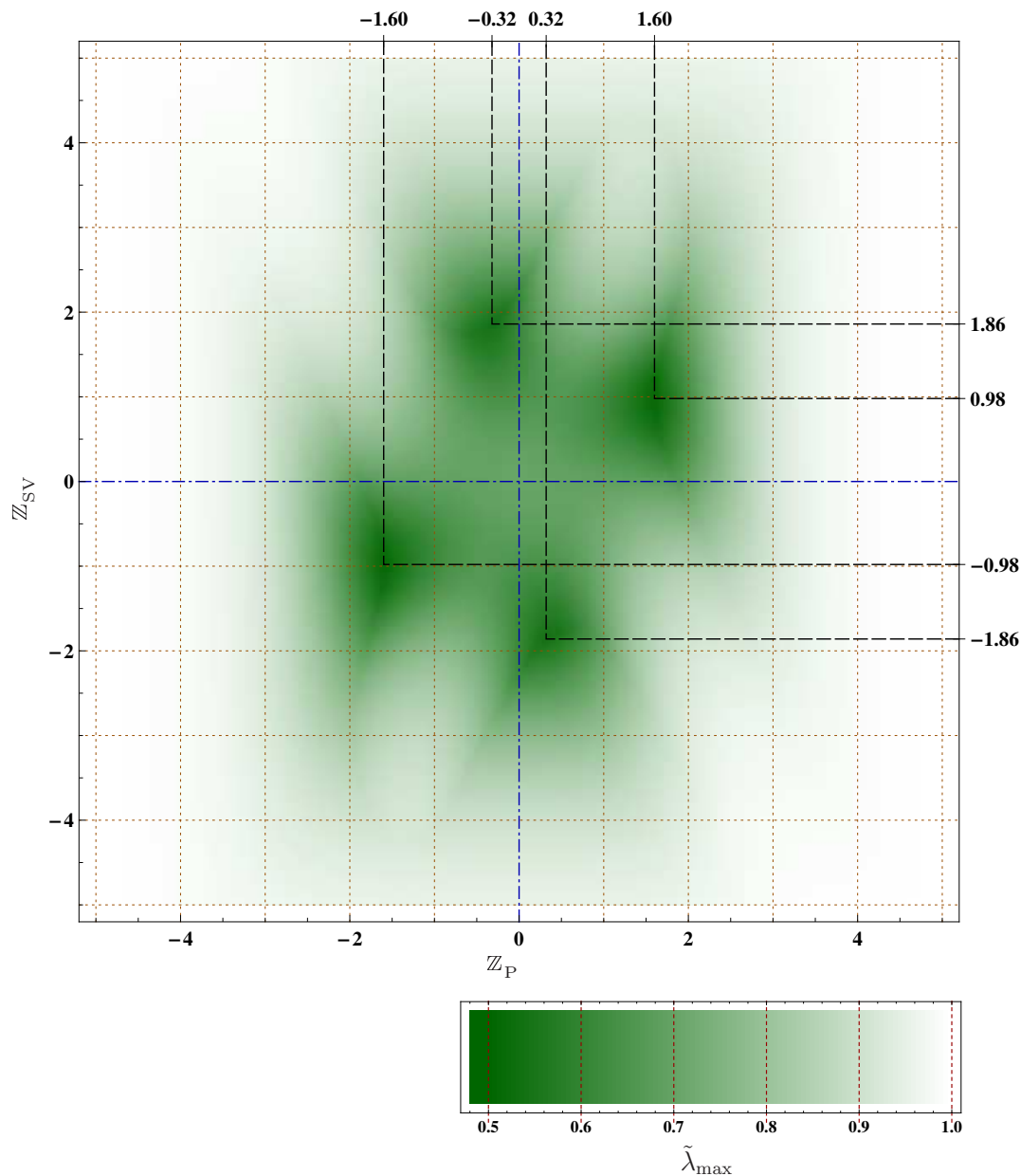


Figure 6:  $\tilde{\lambda}_{\max}$ , the maximum of the absolute values of the matrix  $\tilde{\mathcal{R}}_{\text{top}} \tilde{\mathcal{R}}_{\text{bot}}$ , with respect to the dimensionless origins  $z_P$  and  $z_{SV}$ , for an angle of incidence of  $34^\circ$  and a dimensionless half-thickness  $h=2$ .

The absolute minimum  $\tilde{\lambda}_{\max} \approx 0.51$  is reached for  $z_P \approx \pm 1.6$  and  $z_{SV} \approx \pm 0.98$ .

A local minimum  $\tilde{\lambda}_{\max} \approx 0.54$  appears for  $z_P \approx \pm 0.32$  and  $z_{SV} \approx \mp 1.86$ .  $\tilde{\lambda}_{\max} \approx 0.70$  for  $z_P = 0$  and  $z_{SV} = 0$ .

energy repartition between the two P- and SV-modes depends then on the inhomogeneous mode basis. Indeed, close to the Rayleigh angle, this energy repartition varies very rapidly in less than  $0.2^\circ$  of angle variation, the energy is totally transmitted either to the P-mode at the left hand side or to the SV-mode at the right hand side (see Fig. 8-c).

In the case where the  $z$ -origins are chosen such that the symmetry of the problem is preserved, *i.e.*  $z_{SV,P} = 0$  and  $\delta h_{SV,P} = h$ , the reflection and transmission coefficients can be analyzed from Figs. 7-b to 7-d for increasing values of the plate thickness. On the one hand, the reflection coefficient  $\tilde{r}_0$  tends to the classic solution  $r_0$ , and, on the other hand, the transmission coefficients  $\tilde{g}_{0SV}$  and  $\tilde{g}_{0P}$  tend to zero as far as the associated transmitted waves are inhomogeneous. For large values of the  $h$  dimensionless parameter, one component of the wave displacement field at the upper interface, given by Eq. (42), tends to infinity, while the other component tends to zero. The transmitted inhomogeneous waves (sum of two bivectors) tend to the classical inhomogeneous waves (one bivector). The reflected (or transmitted) energy is then equal to unity (or zero).

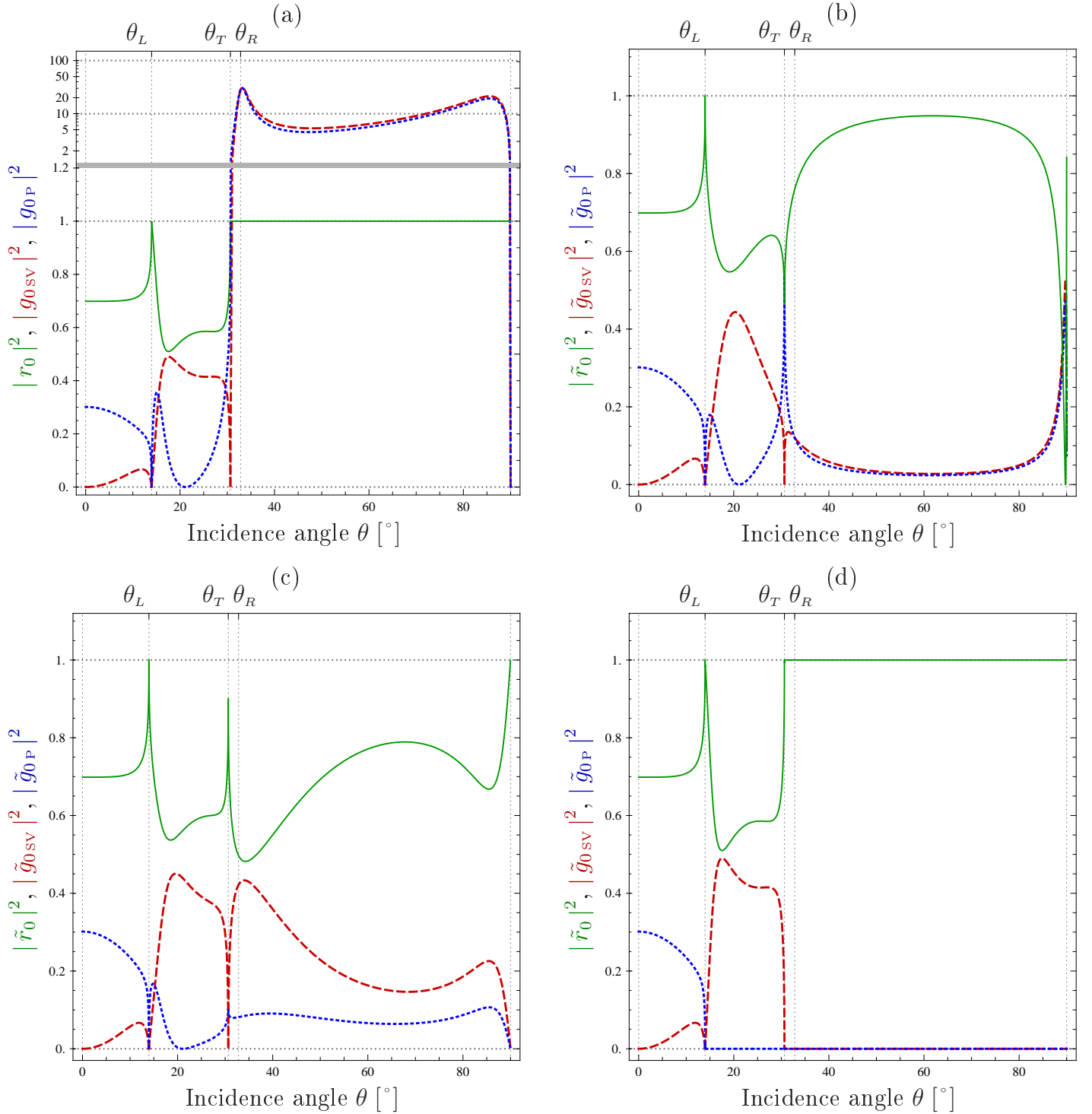


Figure 7: The first reflection/refraction at the upper interface. (a) Square of the absolute values of the reflection coefficient  $r_0$  (solid) and of the components  $g_{0SV}$  (dashed) and  $g_{0P}$  (dotted) of the transmission vector  $\mathbf{g}_0 = (g_{0SH}=0, g_{0SV}, g_{0P})^T$  in the exponential basis, considering the interface positioned at  $z = 0$ . The reflection coefficient  $\tilde{r}_0$  and the transmission vector  $\tilde{\mathbf{g}}_0$  in the alternative basis, with the dimensionless relative position of the interface with respect to the  $z$ -origins  $\delta h_{SV} = \delta h_P = \delta h$ , for (b)  $|\delta h| < 0.1$  ( $z$ -origins near the interface), (c)  $\delta h = \pm 1.5$ , and (d)  $|\delta h| > 50$  ( $z$ -origins far from the interface).

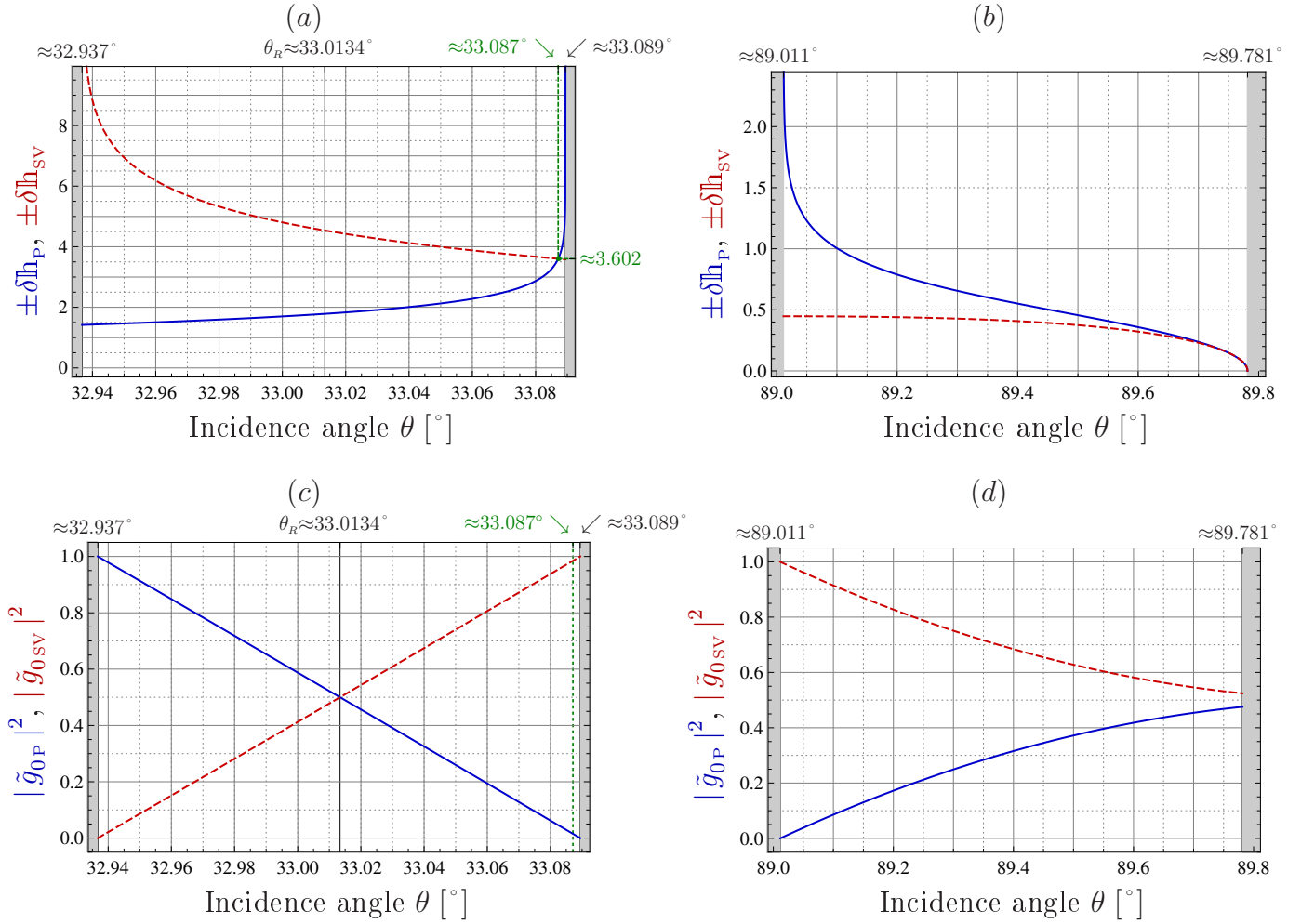


Figure 8: Perfect impedance matching occurs in the two zones (a) ( $32.937^\circ \lesssim \theta \lesssim 33.089^\circ$ ) and (b) ( $89.011^\circ \lesssim \theta \lesssim 89.781^\circ$ ) for specified dimensionless relative positions  $\delta h_{SV}$  (dashed) and  $\delta h_P$  (solid). The reflection coefficient  $\tilde{r}_0$  is zero and the square of the absolute values of the transmission coefficients  $\tilde{g}_{0SV}$  (dashed) and  $\tilde{g}_{0P}$  (solid) are drawn on (c) and (d).

### 4.3 First inner reflections/refractions

To complete the study let us examine the energy repartition between the upgoing and downgoing waves inside the plate. To this end, the absolute values of the coefficients associated with the reflected, transmitted, upgoing and downgoing waves, are plotted on Fig. 9 versus the angles of incidence.

On this figure it is observed first that for the Lamb modes  $S_2$ ,  $S_1$ ,  $A_1$  and  $S_0$ , the upgoing and downgoing energies are both very large. This reveals the existence of strong interferences in the plate, which is the intrinsic nature of guided waves. Such interpretation would not be possible by using the classical inhomogeneous waves in the plate. However, it is of great importance to note that, although this interpretation seems to be very satisfying from a physical point of view, it is determined by the choice of the orthogonal basis referred to in the above discussion. A different choice would provide different relative energies between all the inner waves. Removing this ambiguity merits particular attention and additional efforts remain to be done for a better understanding of this point.

Second, let us focus our interest on the zone close to the Rayleigh angle which corresponds to a perfect matched impedance at the first interface for  $\delta h_{SV,P} = h \approx 3.602$ , as identified on Fig. 8-a at  $\theta \approx 33.087^\circ$ . By comparing the energy repartition between the P- and SV-waves, it is noticeable that the quasi totality of the incident wave energy is transferred to the SV-wave. On the other hand, less than 2% of the energy is transferred to the upgoing waves. This means that the quasi totality of the energy is transmitted in the fluid by the first reflection/refraction at the second interface. For these specific conditions, the plate seems to be transparent, in a sense that all the energy brought by the incident wave in the upper fluid, is totally transmitted in the lower fluid, without any multiple reflections/refractions within the plate.

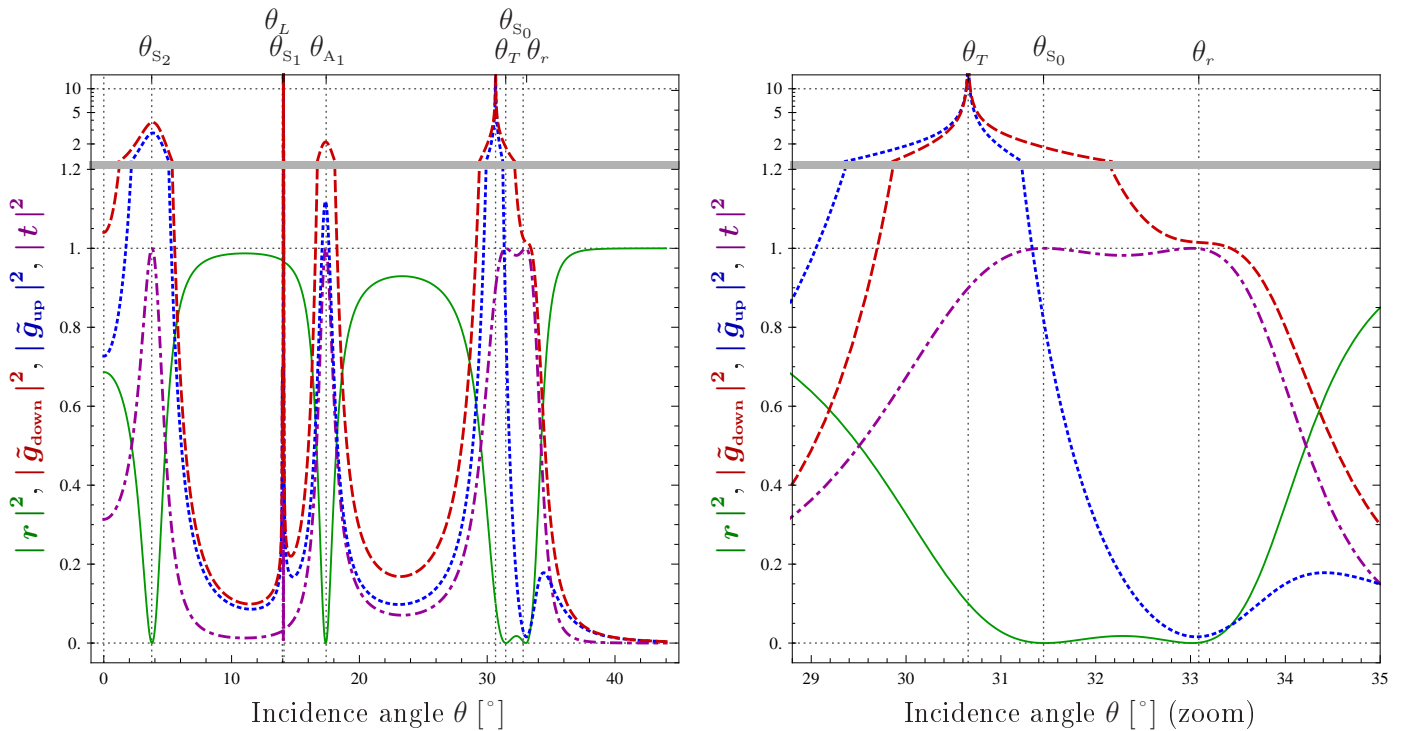


Figure 9: Global coefficients:  $|r|^2$  (reflection, **solid**),  $|t|^2$  (transmission, **dash-dot**),  $|\tilde{\mathbf{g}}_{\text{up}}|^2$  (upgoing energy, **dotted**) and  $|\tilde{\mathbf{g}}_{\text{down}}|^2$  (downgoing energy, **dashed**) for the dimensionless half-thickness  $h \approx 3.602$ , in the orthogonal symmetric basis ( $z_{SV} = z_P = 0$ ).

## 5 Conclusion

The outcome of this study suggests a method to ensure the convergence of the series resulting from the multiple reflections/refractions, which give the total fields reflected and transmitted by an immersed plate. This method is based on the orthogonalization, in the sense of energy, of the basis of solutions formed initially by the harmonic homogeneous (or not) plane waves. When these initial components are inhomogeneous waves, the new basis vectors are composed by the sum of two harmonic inhomogeneous plane waves adequately chosen. Working in this new basis, it has been made clear that the series converges in any situation.

In addition to the systematic convergence of the Debye series, it also has been shown how the speed of this convergence can either increase or decrease by changing the arbitrary origins of the nonstandard inhomogeneous plane waves.

Beyond this obvious improvement of the convergence of the series, an interesting phenomenon has been observed for an aluminum plate immersed in water, for an incidence angle close to the Rayleigh conditions and for a fixed frequency associated to Lamb wave generation. In this case, the plate seems to be really transparent, in a sense that no energy stays in the guide.

Future works should be imagined on the basis of the present results. The extension to immersed solid of other geometries (cylinder, sphere) is a problem which without any doubt can be solved and which will maybe reveal other interesting phenomena, as the transparency of the solid medium. In the case of multiple scattering, when the thermal effects are taken into consideration, the closest objects, spherical or cylindrical most of the time, exchange energy among others interactions through thermal waves (*e.g.*, [24]), these waves being inhomogeneous. The coupling between two objects created by such interactions should be revisited in the light of the work described in this paper.

## Acknowledgments

The authors wish to express their gratitude to Dmitri Zakharov and Alexander Shuvalov for helpful discussions.

## References

- [1] P. Debije, Das elektromagnetische Feld um einen Zylinder und die Theorie des Regenbonens, *Phys. Z.* 9 (1908) 775–778.
- [2] L. M. Brekhovskikh, *Waves in layered media (Applied mathematics and mechanics)*, Academic Press, New York, 1960.
- [3] J. H. M. T. Van Der Hijden, *Propagation of Transient Elastic Waves in Stratified Anisotropic Media (North-Holland Series in Applied Mathematics and Mechanics)*, Elsevier Science Ltd, 1987.
- [4] D. Brill, H. Überall, Acoustic waves transmitted through solid elastic cylinder, *J. Acoust. Soc. Am.* 50 (1971) 921–939.
- [5] J.-M. Conoir, A. Gérard, Un nouveau fond potentiel pour la matrice S, *J. Acoustique* 2 (1989) 217–227.
- [6] A. Gérard, Scattering by spherical elastic layers: Exact solution and interpretation for a scalar field, *J. Acoust. Soc. Am.* 73 (1983) 13–17.

- 
- [7] M. Deschamps, C. Cao, Reflection/refraction of a solid layer by Debye's series expansion, *Ultrasonics* 29 (1991) 288–293.
- [8] J.-M. Conoir, A. Gérard, A. Derem, Ondes acoustiques transmises et séries de Debye généralisées. 1 - traitement des interfaces planes, *J. Acoustique* 4 (1991) 159–200.
- [9] M. Deschamps, B. Hosten, The effects of viscoelasticity on the reflection and transmission of ultrasonic waves by an orthotropic plate, *J. Acoust. Soc. Am.* 91 (1992) 2007–2015.
- [10] A. N. Stroh, Steady state problems in anisotropic elasticity, *J. Math. and Physics* 41 (1962) 77–103.
- [11] J. Lothe, D. M. Barnett, On the existence of surface-wave solutions for anisotropic elastic half-spaces with free surface, *J. Applied Physics* 704 (2) (1976) 428–433.
- [12] P. Chadwick, G. D. Smith, Foundations of the theory of surface waves in anisotropic elastic materials, *Advances in Applied Mechanics* 17 (1977) 303–376.
- [13] T. C. T. Ting, *Anisotropic Elasticity*, no. ISBN 978-0195074475, Oxford University Press, Oxford, 1996.
- [14] A. L. Shuvalov, O. Poncelet, M. Deschamps, Analysis of the dispersion spectrum of fluid-loaded anisotropic plates: flexural-type branches and real-valued loops, *J. Sound Vib.* 290 (2006) 1175–1201.
- [15] A. L. Shuvalov, Theory of plane subsonic elastic waves in fluid-loaded anisotropic plates, *Proc. R. Soc. Lond. A* 458 (2002) 1323–1352.
- [16] V. I. Alshits, G. A. Maugin, Dynamic of multilayers: elastic waves in an anisotropic graded or stratified plate, *Wave Motion* 41 (2005) 357–394.
- [17] V. I. Alshits, J. Lothe, Some basic properties of bulk elastic waves in anisotropic media, *Wave Motion* 40 (2004) 297–313.
- [18] L. E. Pitts, T. J. Plona, W. G. Mayer, Theoretical similarities of Rayleigh and Lamb modes of vibration, *J. Acoust. Soc. Am.* 60 (1976) 374–377.
- [19] D. M. Barnett, J. Lothe, Consideration of the existence of surface wave (Rayleigh wave) solutions in anisotropic elastic crystals, *J. Phys. F: Metal Phys.* 4 (1974) 671–686.
- [20] A. L. Shuvalov, A sextic formalism for three-dimensional elastodynamics of cylindrically anisotropic radially inhomogeneous materials, *Proc. R. Soc. Lond. A* 459 (2003) 1611–1639.
- [21] A. N. Norris, A. L. Shuvalov, Wave impedance matrices for cylindrically anisotropic radially inhomogeneous elastic solids, *Quarterly J. Mech. and Appl. Math.* 63 (2010) 401–435.
- [22] M. Hayes, Inhomogeneous plane waves, *Arch. Rat. Mech. Anal.* 29 (4) (1984) 41–79. doi:10.1007/BF00250866.
- [23] O. Poncelet, M. Deschamps, Lamb waves generated by complex harmonic inhomogeneous plane waves, *J. Acoust. Soc. Am.* 102 (1) (1997) 292–300.
- [24] R. E. Challis, M. J. W. Povey, M. L. Mather, A. K. Holmes, Ultrasound techniques for characterizing colloidal dispersions, *Rep. Prog. Phys.* 68 (2005) 1541–1637.
- [25] J. G. Scholte, On the stoneley wave equation, *Proc. K. Ned. Akad. Wet.* 45 (1942) Pt. 1: 20–25, Pt. 2: 159–164.
- [26] I. A. Viktorov, *Rayleigh and Lamb Waves, Physical Theory and Applications*, Plenum Press, New York, 1967.

# Appendix A Detailed calculations for an isotropic plate

## A.1 The exponential basis

Consider an isotropic plate of density  $\rho_0$ . The slownesses in the  $z$ -direction are:

$$s_1 = s_2 = s_T, \quad s_3 = s_L, \quad s_4 = s_5 = -s_T, \quad s_6 = -s_L, \quad (\text{A.1.a})$$

where

$$s_{L,T} = \begin{cases} \sqrt{\frac{1}{c_{L,T}^2} - s_x^2}, & c_{L,T} s_x < 1, \\ -i \sqrt{s_x^2 - \frac{1}{c_{L,T}^2}}, & c_{L,T} s_x > 1, \end{cases} \quad (\text{A.1.b})$$

$c_L$  and  $c_T$  denoting respectively the longitudinal and transverse velocities.

By using dimensionless slownesses  $\beta = c_T \sin \theta / c$ ,  $\beta_L = c_T s_L$ ,  $\beta_T = c_T s_T$ , and  $\beta_F = c_T \cos \theta / c$ , the polarization matrix  $\Xi$  is expressed as follows to satisfy Eq. (38):

$$\Xi = \sqrt{2} \left( \begin{array}{c|c} \frac{1}{\sqrt{\rho_0 c_T}} \mathbb{I}_3 & \mathbb{O} \\ \hline \mathbb{O} & \sqrt{\rho_0 c_T} \mathbb{I}_3 \end{array} \right) \begin{bmatrix} 0 & \frac{\beta_T}{\sqrt{\beta_T}} & \frac{\beta}{\sqrt{\beta_L}} & 0 & -\frac{\beta_T}{\sqrt{\beta_T^*}} & \frac{\beta}{\sqrt{\beta_L^*}} \\ \frac{1}{\sqrt{\beta_T}} & 0 & 0 & \frac{1}{\sqrt{\beta_T^*}} & 0 & 0 \\ 0 & -\frac{\beta}{\sqrt{\beta_T}} & \frac{\beta_L}{\sqrt{\beta_L}} & 0 & -\frac{\beta}{\sqrt{\beta_T^*}} & -\frac{\beta_L}{\sqrt{\beta_L^*}} \\ \hline 0 & \frac{2\beta^2 - 1}{\sqrt{\beta_T}} & -\frac{2\beta\beta_L}{\sqrt{\beta_L}} & 0 & \frac{2\beta^2 - 1}{\sqrt{\beta_T^*}} & \frac{2\beta\beta_L}{\sqrt{\beta_L^*}} \\ -\frac{\beta_T}{\sqrt{\beta_T}} & 0 & 0 & \frac{\beta_T}{\sqrt{\beta_T^*}} & 0 & 0 \\ 0 & \frac{2\beta\beta_T}{\sqrt{\beta_T}} & \frac{2\beta^2 - 1}{\sqrt{\beta_L}} & 0 & -\frac{2\beta\beta_T}{\sqrt{\beta_T^*}} & \frac{2\beta^2 - 1}{\sqrt{\beta_L^*}} \end{bmatrix}. \quad (\text{A.2})$$

With the notations:

$$\begin{aligned} \mathbf{a} &= \rho \beta_L + \rho_0 \beta_F \left[ (2\beta^2 - 1)^2 - 4\beta^2 \beta_L \beta_T \right], & \mathbf{b} &= \rho \beta_L - \rho_0 \beta_F \left[ (2\beta^2 - 1)^2 - 4\beta^2 \beta_L \beta_T \right], \\ \mathbf{c} &= 4\rho_0 \beta_F \beta (2\beta^2 - 1), & \mathbf{d} &= \rho \beta_L + \rho_0 \beta_F \left[ (2\beta^2 - 1)^2 + 4\beta^2 \beta_L \beta_T \right], \end{aligned} \quad (\text{A.3})$$

and the dimensionless half-thickness of the plate  $h = \omega h / c_T = H / c_T$ , we obtain the following reflection matrices:

$$\mathcal{R}_{\text{top}} = \begin{pmatrix} e^{-i\beta_T h} & 0 & 0 \\ 0 & e^{-i\beta_T h} & 0 \\ 0 & 0 & e^{-i\beta_L h} \end{pmatrix} \begin{pmatrix} \frac{\sqrt{\beta_T^*}}{\sqrt{\beta_T}} & 0 & 0 \\ 0 & -\frac{\sqrt{\beta_T^*}}{\sqrt{\beta_T}} \frac{\mathbf{a}}{\mathbf{d}} & \sqrt{\beta_L} \sqrt{\beta_T^*} \frac{\mathbf{c}}{\mathbf{d}} \\ 0 & -\sqrt{\beta_L^*} \sqrt{\beta_T} \frac{\mathbf{c}}{\mathbf{d}} & \frac{\sqrt{\beta_L^*}}{\sqrt{\beta_L}} \frac{\mathbf{b}}{\mathbf{d}} \end{pmatrix} \begin{pmatrix} e^{-i\beta_T h} & 0 & 0 \\ 0 & e^{-i\beta_T h} & 0 \\ 0 & 0 & e^{-i\beta_L h} \end{pmatrix}, \quad (\text{A.4})$$

and

$$\mathcal{R}_{\text{bot}} = \begin{pmatrix} e^{-i\beta_T h} & 0 & 0 \\ 0 & e^{-i\beta_T h} & 0 \\ 0 & 0 & e^{-i\beta_L h} \end{pmatrix} \begin{pmatrix} \frac{\sqrt{\beta_T}}{\sqrt{\beta_T^*}} & 0 & 0 \\ 0 & -\frac{\sqrt{\beta_T}}{\sqrt{\beta_T^*}} \frac{\mathbf{a}}{\mathbf{d}} & -\beta_L \frac{\sqrt{\beta_T}}{\sqrt{\beta_L^*}} \frac{\mathbf{c}}{\mathbf{d}} \\ 0 & \beta_T \frac{\sqrt{\beta_L}}{\sqrt{\beta_T^*}} \frac{\mathbf{c}}{\mathbf{d}} & \frac{\sqrt{\beta_L}}{\sqrt{\beta_L^*}} \frac{\mathbf{b}}{\mathbf{d}} \end{pmatrix} \begin{pmatrix} e^{-i\beta_T h} & 0 & 0 \\ 0 & e^{-i\beta_T h} & 0 \\ 0 & 0 & e^{-i\beta_L h} \end{pmatrix}. \quad (\text{A.5})$$

Note that the complex slownesses  $\beta$  such that the denominator  $\mathfrak{d}$  is zero are associated to the leaky Rayleigh wave and to the Scholte wave ([25] and *e.g.*, [26]).

The (1,1)-coefficient in the last two matrices corresponds to the SH wave which interacts neither with the P and SV waves in the plate nor with the acoustic wave in the surrounding fluid. The corresponding eigenvalues are  $\pm \exp(-2 \mathfrak{i} \beta_T \mathfrak{h})$ . The convergence study made in this paper focuses on the P, SV and acoustic waves which are interacting, *i.e.* on the two-by-two bottom-right blocks of the last two matrices.

## A.2 Description of nonstandard progressive waves in isotropic elastic materials

In isotropic materials, the slowness in the  $z$ -direction is either real or imaginary, depending on whether the angle of incidence is greater or less than the first critical angle [or whether the slowness in the  $xy$ -plane is greater or less than the cut-off value, Eq. (A.1)].

If the slowness in the  $z$ -direction is imaginary, we obtain dimensionless attenuation coefficients  $\gamma_{L,T} = c_T \sqrt{s_x^2 - 1/c_{L,T}^2}$  ( $s_x = \sin\theta/c$ ) and the nonstandard progressive inhomogeneous waves are characterized by the following normalized polarization vectors  $\tilde{\mathbf{v}}$  and Poynting vectors  $\tilde{\mathcal{P}}$ , from Eqs. (41), (42) and (A.2), with the  $z$ -origins  $z_{\text{SH}}$ ,  $z_{\text{SV}}$  and  $z_{\text{P}}$ , which can be different for each type of wave:

### SH waves

$$\tilde{\mathbf{v}}_1(\mathbb{z}) = \sqrt{\frac{2}{\rho_0 c_T \gamma_T}} \begin{bmatrix} 0 \\ \cosh(\gamma_T \delta z_{\text{SH}}) - \mathfrak{i} \sinh(\gamma_T \delta z_{\text{SH}}) \\ 0 \end{bmatrix}, \quad (\text{A.6.a})$$

where  $\mathbb{z}$  is the dimensionless position  $\omega z / c_T$  and  $\delta z_{\text{SH}}$  the relative dimensionless position  $\omega (z - z_{\text{SH}}) / c_T$  with respect to the origin  $z_{\text{SH}}$ ,

$$\tilde{\mathbf{v}}_4(\mathbb{z}) = -\mathfrak{i} \sqrt{\frac{2}{\rho_0 c_T \gamma_T}} \begin{bmatrix} 0 \\ \cosh(\gamma_T \delta z_{\text{SH}}) + \mathfrak{i} \sinh(\gamma_T \delta z_{\text{SH}}) \\ 0 \end{bmatrix}, \quad (\text{A.6.b})$$

and

$$\tilde{\mathcal{P}}_{1,4}(\mathbb{z}) = \begin{bmatrix} \frac{c_T s_x}{\gamma_T} \cosh(2 \gamma_T \delta z_{\text{SH}}) \\ 0 \\ \pm 1 \end{bmatrix}. \quad (\text{A.7})$$

### SV waves

$$\tilde{\mathbf{v}}_2(\mathbb{z}) = \sqrt{\frac{2}{\rho_0 c_T \gamma_T}} \left\{ \begin{array}{c} \gamma_T [\cosh(\gamma_T \delta z_{\text{SV}}) + \mathfrak{i} \sinh(\gamma_T \delta z_{\text{SV}})] \\ 0 \\ -c_T s_x [\cosh(\gamma_T \delta z_{\text{SV}}) - \mathfrak{i} \sinh(\gamma_T \delta z_{\text{SV}})] \end{array} \right\}, \quad (\text{A.8.a})$$

$$\tilde{\mathbf{v}}_5(\mathbb{z}) = \mathfrak{i} \sqrt{\frac{2}{\rho_0 c_T \gamma_T}} \left\{ \begin{array}{c} \gamma_T [\cosh(\gamma_T \delta z_{\text{SV}}) - \mathfrak{i} \sinh(\gamma_T \delta z_{\text{SV}})] \\ 0 \\ c_T s_x [\cosh(\gamma_T \delta z_{\text{SV}}) + \mathfrak{i} \sinh(\gamma_T \delta z_{\text{SV}})] \end{array} \right\}, \quad (\text{A.8.b})$$

and

$$\tilde{\mathcal{P}}_{2,5}(\mathbb{z}) = \begin{bmatrix} \frac{c_T s_x}{\gamma_T} \cosh(2 \gamma_T \delta z_{\text{SV}}) (1 + 4 \gamma_T^2) \\ 0 \\ \pm 1 \end{bmatrix}. \quad (\text{A.9})$$

**P waves**

$$\tilde{\mathbf{v}}_3(\mathbf{z}) = \sqrt{\frac{2}{\rho_0 c_T \gamma_L}} \begin{Bmatrix} c_T s_x [\cosh(\gamma_L \delta z_P) - i \sinh(\gamma_L \delta z_P)] \\ 0 \\ \gamma_L [\cosh(\gamma_L \delta z_P) + i \sinh(\gamma_L \delta z_P)] \end{Bmatrix}, \quad (\text{A.10.a})$$

$$\tilde{\mathbf{v}}_6(\mathbf{z}) = i \sqrt{\frac{2}{\rho_0 c_T \gamma_L}} \begin{Bmatrix} -c_T s_x [\cosh(\gamma_L \delta z_P) + i \sinh(\gamma_L \delta z_P)] \\ 0 \\ \gamma_L [\cosh(\gamma_L \delta z_P) - i \sinh(\gamma_L \delta z_P)] \end{Bmatrix}. \quad (\text{A.10.b})$$

and

$$\tilde{\mathcal{P}}_{3,6}(\mathbf{z}) = \begin{bmatrix} \frac{c_T s_x}{\gamma_L} \cosh(2 \gamma_L \delta z_P) (1 + 4 \gamma_L^2) \\ 0 \\ \pm 1 \end{bmatrix}. \quad (\text{A.11})$$

**A.3 Reflection and transmission coefficients at the first interface for nonstandard progressive waves**

Only the case  $\theta > \theta_T$  is treated here and in the next section (both the P-waves and the SV-waves are inhomogeneous), with the relative dimensionless positions  $\delta h_P = \omega (h - z_P) / c_T$  and  $\delta h_{SV} = \omega (h - z_{SV}) / c_T$  and the following positive coefficients:

$$\mathbb{l} = (2\beta^2 - 1)^2; \quad \mathbb{m} = 4\beta^2 \gamma_L \gamma_T; \quad \mathbb{n} = \frac{\rho \gamma_L}{\rho_0 \beta_F}, \quad \mathbb{X} = \exp(-2 \gamma_L \delta h_P) \quad \text{and} \quad \mathbb{Y} = \exp(-2 \gamma_T \delta h_{SV}). \quad (\text{A.12})$$

*Reflection coefficient  $\tilde{r}_0$* 

$$\tilde{r}_0(\mathbb{X}, \mathbb{Y}) = \frac{(\mathbb{l} - \mathbb{m})(\mathbb{X} \mathbb{Y} - 1) + \mathbb{n}(\mathbb{X} - \mathbb{Y}) + i [(\mathbb{l} + \mathbb{m})(\mathbb{X} + \mathbb{Y}) - \mathbb{n}(\mathbb{X} \mathbb{Y} + 1)]}{(\mathbb{l} - \mathbb{m})(\mathbb{X} \mathbb{Y} - 1) - \mathbb{n}(\mathbb{X} - \mathbb{Y}) + i [(\mathbb{l} + \mathbb{m})(\mathbb{X} + \mathbb{Y}) + \mathbb{n}(\mathbb{X} \mathbb{Y} + 1)]}. \quad (\text{A.13})$$

*Transmission coefficient  $\tilde{g}_{0P}$* 

$$\tilde{g}_{0P}(\mathbb{X}, \mathbb{Y}) = \frac{2 \sqrt{\mathbb{l} \mathbb{n} \mathbb{X}} (1 + \mathbb{Y}) + i [2 \sqrt{\mathbb{l} \mathbb{n} \mathbb{X}} (1 - \mathbb{Y})]}{(\mathbb{l} - \mathbb{m})(\mathbb{X} \mathbb{Y} - 1) - \mathbb{n}(\mathbb{X} - \mathbb{Y}) + i [(\mathbb{l} + \mathbb{m})(\mathbb{X} + \mathbb{Y}) + \mathbb{n}(\mathbb{X} \mathbb{Y} + 1)]}. \quad (\text{A.14})$$

*Transmission coefficient  $\tilde{g}_{0SV}$* 

$$\tilde{g}_{0SV}(\mathbb{X}, \mathbb{Y}) = \frac{-2 \sqrt{\mathbb{m} \mathbb{n} \mathbb{Y}} (\mathbb{X} + 1) + i [-2 \sqrt{\mathbb{m} \mathbb{n} \mathbb{Y}} (\mathbb{X} - 1)]}{(\mathbb{l} - \mathbb{m})(\mathbb{X} \mathbb{Y} - 1) - \mathbb{n}(\mathbb{X} - \mathbb{Y}) + i [(\mathbb{l} + \mathbb{m})(\mathbb{X} + \mathbb{Y}) + \mathbb{n}(\mathbb{X} \mathbb{Y} + 1)]}. \quad (\text{A.15})$$

**Symmetries**

$\mathbb{X}^{-1} = \exp(+2 \gamma_L \delta h_P)$  and  $\mathbb{Y}^{-1} = \exp(+2 \gamma_T \delta h_{SV})$  correspond to a symmetry with respect to  $\mathbf{z} = \mathbb{h}$  and:

$$\tilde{r}_0(\mathbb{X}^{-1}, \mathbb{Y}^{-1}) = \tilde{r}_0(\mathbb{X}, \mathbb{Y})^*; \quad \tilde{g}_{0P}(\mathbb{X}^{-1}, \mathbb{Y}^{-1}) = -\tilde{g}_{0P}(\mathbb{X}, \mathbb{Y})^* \quad \text{and} \quad \tilde{g}_{0SV}(\mathbb{X}^{-1}, \mathbb{Y}^{-1}) = -\tilde{g}_{0SV}(\mathbb{X}, \mathbb{Y})^* \quad (\text{A.16})$$

## Perfect impedance matching ( $\tilde{r}_0 = 0$ )

There is uniqueness, up to sign, of the dimensionless positions  $\delta h_p$  and  $\delta h_{sv}$  such that the first reflection is zero [Eq. (A.13)]:

$$\begin{aligned}\delta h_p &= \pm \frac{1}{2\gamma_L} \log \left\{ \frac{2\mathbb{l}n + \sqrt{[(\mathbb{l}+m)^2 - n^2][n^2 - (\mathbb{l}-m)^2]}}{n^2 - (m^2 - \mathbb{l}^2)} \right\} \\ \delta h_{sv} &= \pm \frac{1}{2\gamma_T} \log \left\{ \frac{2mn + \sqrt{[(\mathbb{l}+m)^2 - n^2][n^2 - (\mathbb{l}-m)^2]}}{n^2 - (\mathbb{l}^2 - m^2)} \right\}\end{aligned}\quad (\text{A.17})$$

with the condition of existence:  $\mathbb{l} + m > n$  and  $-n^2 < \mathbb{l}^2 - m^2 < n^2$ .

Note that  $\mathbb{l}^2 - m^2 = (2\beta^2 - 1)^4 - (4\beta^2\gamma_L\gamma_T)^2$  is the Rayleigh polynomial and that the solution of  $\mathbb{l} = m$  corresponds to the Rayleigh wave (in vacuum).

## A.4 Reflection and transmission coefficients for nonstandard progressive waves

The relative dimensionless positions are  $\delta h_p = \omega(h - z_p) / c_T$ ,  $\delta h_{sv} = \omega(h - z_{sv}) / c_T$  for the upper interface and  $\delta h_p = \omega(-h - z_p) / c_T$ ,  $\delta h_{sv} = \omega(-h - z_{sv}) / c_T$  for the lower interface.

*Reflection coefficient  $\tilde{r}_{svsv}^{\text{top,bot}}$*

$$\tilde{r}_{svsv}^{\text{top,bot}}(\mathbb{X}, \mathbb{Y}) = \frac{(\mathbb{l} - m)(\mathbb{X}\mathbb{Y} + 1) + n(\mathbb{Y} + \mathbb{X}) \pm i[(\mathbb{l} + m)(\mathbb{Y} - \mathbb{X}) + n(\mathbb{X}\mathbb{Y} - 1)]}{(\mathbb{l} - m)(\mathbb{X}\mathbb{Y} - 1) + n(\mathbb{Y} - \mathbb{X}) \pm i[(\mathbb{l} + m)(\mathbb{Y} + \mathbb{X}) + n(\mathbb{X}\mathbb{Y} + 1)]}. \quad (\text{A.18})$$

*Reflection coefficients  $\tilde{r}_{psv}^{\text{top,bot}}$ ,  $\tilde{r}_{svp}^{\text{top,bot}}$*

$$\tilde{r}_{psv}^{\text{top,bot}}(\mathbb{X}, \mathbb{Y}) = -\tilde{r}_{svp}^{\text{top,bot}}(\mathbb{X}, \mathbb{Y}) = \frac{\pm 4\sqrt{\mathbb{l}m\mathbb{X}\mathbb{Y}}}{(\mathbb{l} - m)(\mathbb{X}\mathbb{Y} - 1) + n(\mathbb{Y} - \mathbb{X}) \pm i[(\mathbb{l} + m)(\mathbb{Y} + \mathbb{X}) + n(\mathbb{X}\mathbb{Y} + 1)]}. \quad (\text{A.19})$$

*Reflection coefficient  $\tilde{r}_{pp}^{\text{top,bot}}$*

$$\tilde{r}_{pp}^{\text{top,bot}}(\mathbb{X}, \mathbb{Y}) = \frac{(\mathbb{l} - m)(\mathbb{X}\mathbb{Y} + 1) - n(\mathbb{Y} + \mathbb{X}) \pm i[(\mathbb{l} + m)(-\mathbb{Y} + \mathbb{X}) + n(\mathbb{X}\mathbb{Y} - 1)]}{(\mathbb{l} - m)(\mathbb{X}\mathbb{Y} - 1) + n(\mathbb{Y} - \mathbb{X}) \pm i[(\mathbb{l} + m)(\mathbb{Y} + \mathbb{X}) + n(\mathbb{X}\mathbb{Y} + 1)]}. \quad (\text{A.20})$$

*Transmission coefficients:  $\tilde{t}_{sv}^{\text{top}} = i\tilde{g}_{0sv}$ ;  $\tilde{t}_{sv}^{\text{bot}} = \tilde{g}_{0sv}^*$ ;  $\tilde{t}_p^{\text{top}} = -i\tilde{g}_{0p}$ ;  $\tilde{t}_p^{\text{bot}} = \tilde{g}_{0p}^*$ .*